FOLDABLE STRUCTURE BASED ON ORIGAMI WITH CURVED FOLD LINES CONCEPT

NG WAI KEUN

UNIVERSITI SAINS MALAYSIA

2018

FOLDABLE STRUCTURE BASED ON ORIGAMI WITH CURVED FOLD LINES CONCEPT

by

NG WAI KEUN

Thesis submitted in fulfilment of the requirements for the degree of Doctor of Philosophy

August 2018

ACKNOWLEDGEMENT

Nowadays we cannot be separated from the use of paper in our daily life, but very few try to learn from folding this object for possible application related to their discipline. Assoc. Prof. Ir. Dr. Choong Kok Keong, my supervisor, is the man behind the beautiful idea of this research. Thence, I would like to take this opportunity to express my utmost gratitude to Dr. Choong for his invaluable advice, constant guidance, time spent, and patient throughout my entire period of time in completing the research project. I admire his professional style at both academic as well as the personal level.

My appreciation also go to my co-supervisor, Assoc. Prof. Dr. Neeraj Bhardwaj, from College of Computer and Information Sciences, Majmaah University, Saudi Arabia.

I would like to thanks to School of Civil Engineering, Universiti Sains Malaysia, lecturer and staff from who contribute a lot of their strength in this project. Support in the form of MyPhD financing by Ministry of High Education Malaysia is also acknowledged.

Lastly, I owe my loving thanks to my family. They have lost a lot due to my research work. Without their encouragement and understanding it would have been impossible for me to finish this study work.

TABLE OF CONTENTS

	Page
ACKNOWLEDGEMENT	ii
TABLE OF CONTENTS	iii
LIST OF TABLES	ix
LIST OF FIGURES	xi
LIST OF ABBREVIATIONS	xxx
LIST OF SYMBOLS	xxxi
ABSTRAK	xxxiii
ABSTRACT	xxxv

CHAPTER ONE: INTRODUCTION

1.1 General 1
1.2 Background of Study 2
1.2.1 Roof Structures with Folded Shell System 6
1.2.2 Roof Structures with Foldable Design 10
1.3 Structures Inspired from the Geometry of Origami 14
1.4 Justification of Research 19
1.5 Problem Statement 22
1.6 Research Objectives 26
1.7 Scope of Research 27
1.8 Thesis Layout 28

CHAPTER TWO: LITERATURE REVIEW

2.1 Shell Structures 30
2.1.1 Types of shell structures 31
2.1.2 Behaviors of Shell Structures 33
2.2 Folded Surface/Plate Structure 35
2.2.1 Types of Folded Surface/Plate Structures 38
2.2.2 Behaviors of Folded Plate/Surface Structures 40
2.3 Foldable/Retractable Structure 43

2.3.1 Typology of Retractable/Foldable Structures 43
2.3.2 Folding Mechanism of Retractable/Foldable Structures 46
2.4 Past Research Works 52
2.4.1 Past Research Works on Shell and Folded Surface/Plate Structure that Inspired from Origami 52
2.4.2 Past Research Works on Foldable/Retractable Structures that Inspired from Origami 54
2.4.3 Past Research Works on Origami with Curved Fold Lines 57
2.5 3-D Surface Data Acquisition Methods 61
2.5.1 Image Capturing Method – Conventional Approach 63
2.5.2 Structural Lighting Method 64
2.6 Summary 66

CHAPTER THREE: METHODOLOGY

3.1 Introduction 69
3.2 Collection of Origami Models with Curved Fold Lines 70
3.3 Classification of Origami with Curved Fold Lines 83
3.4 Selection of Origami with Curved Fold Lines 84
3.5 Reconstruction of Prototype of Origami Models with Curved Fold Lines 85
3.5.1 Generation for the Plan Configuration of Origami Models 85
3.5.2 Paper Material in Constructing Origami Models 101
3.5.3 Procedures in Generating Origami Paper Models 102
3.5.4 Supporting Points During the Folding Process 103
3.6 3-D Surface Data Acquisition for Origami Model with Curved Fold Lines 109
3.6.1 Image Capturing Method – Conventional Approach 110
3.6.1(a) 3-D Surface Data Measurement Experimental Setup for ICM 110
3.6.1(b) 2-D Outline Generation from the Images 114
3.6.1(c) Definition of External Coordinate System 118
3.6.1(d) Procedures in 3-D Outlines Generation by ICM 120
3.6.1(e) Summary of ICM 127
3.6.2 Structural Lighting Method 128
3.6.2(a) Concept of 3-D Surface Data Acquisition by SLM 128

3.6.2(b) Instrument Setup for DAVID SLS-1 Structured-Light Scanner 131
3.6.2(c) Post Processing of Raw Data of 3-D Image 136
3.6.2(d) Accuracy Verification for 3-D Images Obtained by SLM 141
3.6.2(e) 3-D Model Generation from the Raw Data of SLM 145
3.6.2(f) Sub-surface Division for 3-D Model Generation 148
3.6.2(g) Surface Mesh Generation for 3-D Origami Models 150
3.6.2(h) Summary of SLM 153
3.7 Determination of Folding Mechanism for Origami with Curved Fold Lines 154
3.8 Generation of Finite Element Model for Structural Analysis 156
3.8.1 Surface Element Type and Surface Mesh 157
3.8.2 Geometric Properties of Thin Shell Surface 162
3.8.3 Boundary Condition of Origami Space Structure 166
3.8.4 Loading 170
3.8.5 Material Properties 171
3.9 Summary 171

CHAPTER FOUR: RESULTS AND DISCUSSION

4.1 Results for the Classification of Origami with Curved Fold Lines 175
4.2 Three Dimensional Origami Surface Data Acquisition and Model Generation 182
4.2.1 Data Acquisition by Image Capturing Method (ICM) 182
4.2.1(a) 2-D Images of Origami Models by ICM 183
4.2.1(b) Outline Generation for Origami Models by ICM 188
4.2.2 Data Acquisition by Structural Lighting Method (SLM) 192
4.2.2(a) Raw 3-D Triangulation Mesh Data for the Origami Models by SLM 192
4.2.2(b) Outline Generation for the Origami by SLM 197
4.2.2(c) Outlines Generation with Sub-surface Division for the Origami Models by SLM 202
4.2.2(d) Mesh Generation of the 3-D Origami Models using Data from SLM 207
4.2.3 Discussion of Three-Dimensional Surface Data Acquisition for Origami Models with Curved Fold Lines 212

4.3 Determination of Folding Mechanism for Origami with Curved Fold Lines 214

4.3.1 Folding Mechanism for Origami Models Under Category of Non-inflated *n* Degree-*n* Vertices 215

4.3.1(a) Origami Model A01 – Single Degree-4 Vertices 215

4.3.1(a)(i) Overall Folding Process 221

4.3.1(a)(ii) Change in Configuration of Boundary during Folding Process 224

4.3.1(a)(iii) Change in Configuration of Curved Fold Lines during Folding Process 229

4.3.1(a)(iv) Summary of Folding Mechanism for Origami Model A01 237

4.3.1(b) Summary for Folding Mechanism of Origami Models Under Category A (Non-inflated n Degree-n Vertices) 239

4.3.2 Folding Mechanism for Origami Models Under Category of Inflated *n* Degree-*n* Vertices 243

4.3.2(a) Origami Model B04 – Degree-4 Vertices Inflated into Two Degree-3 Vertices 243

4.3.2(a)(i) Overall Folding Process 249

4.3.2(a)(ii) Change in Configuration of Boundary during Folding Process 254

4.3.2(a)(iii) Change in Configuration of Curved Fold Lines during Folding Process 257

4.3.2(a)(iv) Summary of Folding Mechanism for Origami Model B04 266

4.3.2(b) Summary of Folding Mechanism for Origami Models Under Category B (Inflated n Degree-n Vertices) 267

4.3.3 Folding Mechanism for Origami Models Under Category of Mountain Ridge Curve 272

4.3.3(a) Origami Model C08 – Two Circular Mountain Ridge Curves in Square 272

4.3.3(a)(i) Overall Folding Process 278

4.3.3(a)(ii) Change in Configuration of Boundary during Folding Process 281

4.3.3(a)(iii) Change in Configuration of Curved Fold Lines during Folding Process 286

4.3.3(a)(iv) Summary of Folding Mechanism for Origami Model C08 290

4.3.3(b) Summary for Folding Mechanism of Origami Models Under Category C (Mountain Ridge Curve) 291

4.3.4 Folding Mechanism for Origami Models Under Category of Complex Shape 296

4.3.4(a) Origami Model D13 – 4-Lobed Cloverleaf Design 296

4.3.4(a)(i) Overall Folding Process 301

4.3.4(a)(ii) Change in Configuration of Boundary during Folding Process 304

4.3.4(a)(iii) Change in Configuration of Curved Fold Lines during Folding Process 309

4.3.4(a)(iv) Summary of Folding Mechanism for Origami Model D13 312

4.3.4(b) Summary for Folding Mechanism of Origami Model Under Category D (Complex Shape) 313

4.3.5 Discussion for the Determination of Folding Mechanism for Origami with Curved Fold Lines 317

4.4 Results of Finite Element Modeling and Analysis for Shell Structure with Curved Fold Lines (SSCFL) 319

4.4.1 Introduction 319

4.4.2 Results of Stress Resultants and Moment Resultants for Shell Structure with Curved Fold Lines (SSCFL) 320

4.4.2(a) Stress Resultants 320

4.4.2(b) Moment Resultants 339

4.4.3 Results of Displacement on Shell Structure with Curved Fold Lines (SSCFL) 359

4.4.3(a) SSFCL Based on Origami Model C11 – Five Circular Mountain Ridge Curves in Pentagon 360

4.4.3(b) SSFCL Based on Origami Model C12 – Four Elliptical Mountain Ridge Curves in Octagon 366

4.4.3(c) SSFCL Based on Origami Model D13 – 4-Lobed Cloverleaf Design 371

4.4.3(d) Effects of Pattern of Curved Fold Lines on Shell Surface Structure 376

4.5 Summary 378

CHAPTER FIVE: CONCLUSIONS AND RECOMMENDATIONS

5.1 Conclusions 379

5.2 Recommendations for Future Works 382

REFERENCES 383

APPENDICES

Appendix A: 2-D Images (Top View) of Origami Models by ICM
Appendix B: 2-D Images (Side View) of Origami Models by ICM
Appendix C: Outlines Generation (Plan View) of Origami Models by ICM
Appendix D: Outlines Generation (Side View) of Origami Models by ICM
Appendix E: Outlines Generation (3-D View) of Origami Models by ICM
Appendix F: Raw Data of 3-D Triangulation Mesh for the Origami Models by SLM (3-D View)
Appendix G: Outlines Generation with Sub-surface Division for the Origami Models by SLM (3-D View)
Appendix H: Surface Mesh Generation for the Origami Models by SLM (3-D View)
Appendix I: Folding Mechanism of Origami Model A02 – Two Degree-2 Vertices
Appendix J: Folding Mechanism of Origami Model A03 – Four Degree-4 Vertices
Appendix K: Folding Mechanism of Origami Model B05 – Degree-4 Vertices Inflated into Four Degree-3 Vertices
Appendix L: Folding Mechanism of Origami Model B06 – Degree-4 Vertices Inflated into Four Degree-3 Vertices (with Inner Square Oriented 45° from *X*-axis)
Appendix M: Folding Mechanism of Origami Model B07 – Degree-6 Vertices Inflated into Six Degree-3 Vertices
Appendix N: Folding Mechanism of Origami Model C09 – Four Circular Mountain Ridge Curves in Square
Appendix O: Folding Mechanism of Origami Model C10 – Four Elliptical Mountain Ridge Curves in Square
Appendix P: Folding Mechanism of Origami Model C11 – Five Circular Mountain Ridge Curves in Pentagon
Appendix Q: Folding Mechanism of Origami Model C12 – Four Elliptical Mountain Ridge Curves in Octagon
Appendix R: Contour Diagrams of Stress Resultants for Origami Model C09
Appendix S: Contour Diagrams of Stress Resultants for Origami Model C12
Appendix T: Contour Diagrams of Moment Resultants for Origami Model C12

LIST OF PUBLICATIONS

LIST OF TABLES

		Page
Table 3.1	List of Collections of Origami Models with Curved Fold Lines	73
Table 3.2	Plan Geometrical Details for Origami Model A01	89
Table 3.3	Plan Geometrical Details for Origami Model A02	90
Table 3.4	Plan Geometrical Details for Origami Model A03	91
Table 3.5	Plan Geometrical Details for Origami Model B04	92
Table 3.6	Plan Geometrical Details for Origami Model B05	93
Table 3.7	Plan Geometrical Details for Origami Model B06	94
Table 3.8	Plan Geometrical Details for Origami Model B07	95
Table 3.9	Plan Geometrical Details for Origami Model C08	96
Table 3.10	Plan Geometrical Details for Origami Model C09	97
Table 3.11	Plan Geometrical Details for Origami Model C10	97
Table 3.12	Plan Geometrical Details for Origami Model C11	98
Table 3.13	Plan Geometrical Details for Origami Model C12	99
Table 3.14	Plan Geometrical Details for Origami Model D13	100
Table 3.15	Detail Information of the Fold Stages during Folding Process	106
Table 3.16	Details for the Direction of Measurement for each Individual Lines	122
Table 3.17	Verification of 3-D Data Obtained by SLM with Actual Measured Surface Length for Specified Shape	144
Table 3.18	Quantitative Parameters of Measurement on Change in Geometry of Origami Model during Folding Process	155
Table 3.19	Historical Statistic of Thin Shell Structures with respect to the Ratio of Span to Thickness	164
Table 3.20	Details of Length of Span between Two Supports with respect to each Folding Stage for Origami Models	169

Table 4.1	Detailed Information for Selected Origami Models with Curved Fold Lines	181
Table 4.2	Number of Folding Stage for Origami Models	185
Table 4.3	Results for the Angular Rotation and Elevation at Center of Origami Model A01	224
Table 4.4	Results of Pixel Analysis for Change in Plan Area during Folding Process of Model A01	228
Table 4.5	Results of Measurement on Length from Centre to the End of Mountain Fold (ℓ_{MF}) for Origami Model A01	234
Table 4.6	Results of Angular Measurement for the Rotation of Mountain Fold (θ_M) for Origami Model A01	234
Table 4.7	Results of Height Measurement for Mountain Folds at Boundary (H_{MB}) during Folding Process for Origami Model A01	236
Table 4.8	Summary for the Results of Parametric Measurements for Origami Models under Category A at Final Folding Stage	239
Table 4.9	Summary for the Results of Parametric Measurements for Origami Models under Category B at Final Folding Stage	268
Table 4.10	Summary for the Results of Parametric Measurements for Origami Models under Category C at Final Folding Stage	293
Table 4.11	Summary for the Results of Parametric Measurements for Origami Models under Category D at Final Folding Stage	314
Table 4.12	Maximum and Minimum Stress Resultant in Local Cartesian for All SSFCL	322
Table 4.13	Stress Resultant Capacity of Compressive, Tensile and Shear for Concrete C30	329
Table 4.14	Allowable Stress Resultant for Concrete	330
Table 4.15	Maximum and Minimum Moment Resultant in Local Cartesian for SSCFL	341
Table 4.16	Capacity of Moment Resultants for Concrete C30	349
Table 4.17	Allowable Moment Resultant in Local *x*, *y*, and *xy* Directions	349
Table 4.18	Maximum Resultant Displacement (RSLT) with respects to the Stage of Folding for SSCFL Models, in comparison to the Allowable Displacement According to BS8110	360

LIST OF FIGURES

		Page
Figure 1.1	Typologies for the Forms of Long Span Roof Structural System	3
Figure 1.2	Successful Application of Long Span Structural System: (a) Space Structure; (b) Cable Structure; (c) Membrane Structure; (d) Hybrid Structure; and (e) Convertible Structure	5
Figure 1.3	Some Applications of Folded Shell Structures	8
Figure 1.4	Some Applications of Foldable Roof Structures	12
Figure 1.5	Type of origami	15
Figure 1.6	Structures Inspired from Geometry of Origami	17
Figure 1.7	Curve Creased Models: (a) by Josef Albers's students; (b) by Irene Schawinsky; (c) by Thoki Yenn; and (d) Kunihiko Kasahara	20
Figure 1.8	Curve Creased Models: (a) "The White Space Curve Fold with 3-fold Symmetry" by Ronald Resch; (b) Two Degree-2 Vertices; (c) Non-Inflated Degree-4 Vertex; and (d) "Hexagonal column with cusps" by Huffman	21
Figure 1.9	Two Examples of origami models with Mountain Ridged Curve Folds by Yoshinobu Miyamoto	22
Figure 1.10	The Development of Research Works in the Context of Form Finding in Origami with Curved Fold Lines	23
Figure 1.11	Folding Process of Origami Surface with Curved Fold Lines from initial opening-stage of (a) to final closed-stage of (d)	24
Figure 2.1	Definition of Curvature for Shell Surface Form: (a) Positive Gaussian; (b) Zero Gaussian; and (c) Negative Gaussian	32
Figure 2.2	Types for the Form of Shell Structures	34
Figure 2.3	In-plane and Out of Plane Forces of Shell Surface Element	36
Figure 2.4	The Stiffness and Load Carrying Capacity of Folded Plate: (a) A piece of Paper without any Fold could not carry Its Own Weight; (b) After being Folded the Paper can Not Only Stand between the Gap, but also carry Some Extra	37

	Weight; (c) When the Load is being Added, the Folded Paper need to be Stiffened; and (d) After the Edges were Stiffened, the Structure could carry More Loads	
Figure 2.5	Typology of Fold Plate Structural Systems	39
Figure 2.6	Loading Distribution for Folded Plate Structure	41
Figure 2.7	Longitudinal Action of Folded Plate Structures	42
Figure 2.8	Transverse Action of Folded Plate Structures	42
Figure 2.9	Types of Deployable Structures	45
Figure 2.10	Types of Retractable Roof Structures for Stadium and Sport Halls: (a) Retractable Roof Structures composed of Rigid Elements; (b) Retractable Roof Structures composed of Membranes; and (c) Retractable Roof Structures composed of Rigid Elements and Membranes	46
Figure 2.11	Folding Mechanism of Retractable/Foldable Structures	48
Figure 2.12	Centric Configuration of Folding Process: (a) Umbrella Structures at Prophet`s Holy Mosque in Madinah; and (b) Open and Close Profile of Transformation Direction	47
Figure 2.13	Linear Configuration of Folding Process: (a) Curved Linkage Bars with Scissor System at Jaén Auditorium in Spain; and (b) Stowed and Employed Stage of Transformation Direction	49
Figure 2.14	Deformable Structure of Floating Theater in Osaka, Japan	50
Figure 2.15	Folding Transformation Strategy for Membrane-cable Folding Structure of National Stadium in Warsaw, Poland	51
Figure 2.16	Rotation Transformation Strategy for Dome Structure of Civic Arena in USA	51
Figure 2.17	Sliding Transformation Strategy for Bi-Parting Rigid Structure of Ariake Colosseum Hall in Japan	52
Figure 3.1	Basis Formation of an Origami with Curved Fold Lines	72
Figure 3.2	Dimensional Limit of Square Space for Origami Modeling	86
Figure 3.3	Procedures in generating Plan Configuration of Origami Model A01	87
Figure 3.4	Plan shape of Origami Model A01	88
Figure 3.5	Plan shape of Origami Model A02	89

Figure 3.6	Plan shape of Origami Model A03	90
Figure 3.7	Plan shape of Origami Model B04	92
Figure 3.8	Plan shape of Origami Model B05	93
Figure 3.9	Plan shape of Origami Model B06	94
Figure 3.10	Plan shape of Origami Model B07	95
Figure 3.11	Plan shape of Origami Model C08	96
Figure 3.12	Plan shape of Origami Model C09	96
Figure 3.13	Plan shape of Origami Model C10	97
Figure 3.14	Plan shape of Origami Model C11	98
Figure 3.15	Plan shape of Origami Model C12	99
Figure 3.16	Plan shape of Origami Model D13	100
Figure 3.17	Manila Card the paper material used in Constructing Origami Models	101
Figure 3.18	Step-by-step Procedures in Folding Origami Paper Model A01: (a) Blank A4-Sized Manila Card Paper, (b) Plan Configuration Printed on the Paper, (c) Square Boundary is Cut Out, (d) Tracing the Crease Lines, (e) Pre-creasing by using Backside of Blade Knife, (f) Mountain Fold, (g) Valley Fold, (h) and (i) Views of Final Finishing Folded Paper Model	104
Figure 3.19	Regeneration of 13 units of Origami Paper Model	105
Figure 3.20	Location of Supporting Points with respect to Folding Stage during entire Folding Process of Origami Models	107
Figure 3.21	Experimental Setup for the Instrument use in ICM	112
Figure 3.22	Experimental Setup for ICM	113
Figure 3.23	Top View Outline (*XY*-plane) Generation based on the 2-D images of Model A02 captured by ICM	116
Figure 3.24	Side View Outline (*XZ*-plane) Generation based on the 2-D images of Model A02 captured by ICM	117
Figure 3.25	Details of Hidden Lines Due to Overlapping of Paper Surfaces during Process of Folding (*Fs*=06) for Top Image of Model A02	115

Figure 3.26	Definition of External Geometrical System for 3-D Model Generation	119
Figure 3.27	Concept of Epipolar Plane and Epipolar Lines used in ICM	121
Figure 3.28	Details of Model A02 with Separation of Individual Lines	122
Figure 3.29	Spacing of Grids used for Measuring Geometrical Profile of Boundary Line *B*1 of Model A02 at *Fs*=01: (a) Top View (*XY*-plane); and (b) Side View (*XZ*-plane)	123
Figure 3.30	Generation of 3-D boundary line *B*1 for Model A02 at *Fs*=01: (a) Building-up of Elevation Profile from the Side View of Outline Plane; and (b) Transferring the Elevation Profile into *XY*-plane	124
Figure 3.31	Generation of 3-D lines of *B*1, *B*2, *F*1 and *F*2 for Model A02 at *Fs*=01	125
Figure 3.32	Complete 3-D Generation for Model A02 at *Fs*=01	125
Figure 3.33	3-D Geometrical Lines Generation for a Combination of folding stages of Origami Model A02: (a) 3-D View; (b) Top View; (c) Front View; and (d) Side View	126
Figure 3.34	Illustration for the Concept of Optical Intersection between Projected Light to the Receiver of Camera by SLM	130
Figure 3.35	Sequence of Binary-coded Pattern Projection for 3-D Imaging by SLM	131
Figure 3.36	Illustration of Instrumental Setup for 3-D Surface Data Acquisition by DAVID SLS-1 Structured Light Scanner	132
Figure 3.37	Instrumental Setup Arrangement for 3-D Surface Data Acquisition by using DAVID SLS-1 Structured-Light Scanner	134
Figure 3.38	Calibration Panel provided by DAVID SLS-1	135
Figure 3.39	Process of Calibration: (a) Camera Calibration; and (b) Projector Calibration	135
Figure 3.40	Rotary Disc Board designed for Multiple Scanning of Origami Model during Later folding Stages by Side Aligned Scanning System	136
Figure 3.41	Raw Data of 3-D Image captured by SLM with Unnecessary Parts of Background and Noise of Disturbance	137

Figure 3.42	Merging Process of Origami Model A03 to form a Complete Surface	139
Figure 3.43	Smoothening of the Raw Data of 3-D Images for Origami Model A01: (a) Effect before Smooth Scan; and (b) Effect after Smooth Scan	140
Figure 3.44	Reduction of Point Cloud Density from Raw Data of 3-D Images for Origami Model A02 at *Fs*=01	141
Figure 3.45	Three Rubik's Polygon selected for Accuracy Verification Test: (a) Cube; (b) Pyramid; and (c) Pentagon	142
Figure 3.46	Measurement of Actual Model and 3-D Scanned Model for the Shapes of: (a) Rubik Cube; (b) Rubik Pyramid and (c) Rubik Pentagon	143
Figure 3.47	Details of Generating Nodes on the Intersection Points between Raw Data and Grid of Reference for Origami Model A01 at *Fs*=01	146
Figure 3.48	Procedures in Generating 3-D Outlines from Raw Data Scanned by SLM for Origami Model A01 at *Fs*=01	147
Figure 3.49	Outlines Plane for Sub-surface Division	148
Figure 3.50	Isometric View of Origami Model A01 at *Fs*=01 after Sub-surface Divisions are Generated	149
Figure 3.51	Surface Meshing Functions provided by CAD Program: (a) EDGESURFT; and (b) RULESURF	151
Figure 3.52	Complete 3-D Model Generation with Surface Meshing for Origami Model A01 at *Fs*=01: (a) 3-D View; (b) Plan View; (c) Front View; and (d) Side View	152
Figure 3.53	Measurement for the Change in Geometry during Folding Process of Origami Model A01	154
Figure 3.54	Finite Element Attributions of Surface Element Type and Surface Meshing for Origami Model A01 at Fs=01: (a) 3-D Surface of Origami Model; (b) Sub-surface with Meshes; and (c) Thin Shell Element	158
Figure 3.55	Surface Meshing Elements in FEM for 13 Origami Models	159
Figure 3.56	Study of Convergence regarding Resultant Displacement due to the Selection of Surface Element Shapes and Degree of Interpolation Order, with respect to the Number of Surface Element Division in Local *X* and Local *Y*	161

	Directions: (a) Folding Stage *Fs*=01 (Start of Folding); and (b) Folding Stage *Fs*=04 (End of Folding), for Model A01	
Figure 3.57	Dimension of Origami Paper Model Scaled to Actual Size of Space Structure	162
Figure 3.58	Surface Thicknesses in FEM for 13 Origami Models	165
Figure 3.59	Attribution of Surface Thicknesses on Finite Element Model A01 at *Fs*=01	166
Figure 3.60	Attribution of Fixed Support on Finite Element Model A01 at *Fs*=01	167
Figure 3.61	Location of Supporting Lines in FEM for 13 Origami Models	168
Figure 3.62	Attribution of Self-weight Loading Applied in FEM for Origami Model A01 at *Fs*=01	170
Figure 3.63	Flowchart of Current Research Study	173
Figure 4.1	Classification of Origami with Curved Fold Lines based on Source of References	176
Figure 4.2	Categories of Origami Model with Curved Fold Lines Selected	180
Figure 4.3	Top View (*X*-*Y* plane) of Origami Model A01 (Degree-4 Vertices) folded from *Fs*=00 (Un-fold Stage) to *Fs*=07 (Final Stage) by Image Capturing Method	186
Figure 4.4	Side View (*Y*-*Z* plane) of Origami Model A01 (Degree-4 Vertices) folded from *Fs*=00 (Un-fold Stage) to *Fs*=04 (Final Stage) by Image Capturing Method	187
Figure 4.5	Outline Generation for Plan View (*X*-*Y* plane) of Origami Model A01 (Degree-4 Vertices) folded from *Fs*=00 (Un-fold Stage) to *Fs*=04 (Final Stage) by Image Capturing Method	189
Figure 4.6	Outline Generation for Side View (*Y*-*Z* plane) of Origami Model A01 (Degree-4 Vertices) folded from *Fs*=00 (Un-fold Stage) to *Fs*=04 (Final Stage) by Image Capturing Method	190
Figure 4.7	Outline Generation for Isometric View (3-D View) of Origami Model A01 (Degree-4 Vertices) folded from *Fs*=00 (Un-fold Stage) to *Fs*=04 (Final Stage) by Image Capturing Method	191

Figure 4.8	Raw 3-D Triangulation Mesh for Origami Model A03 (Four Degree-4 Vertices) folded from *Fs*=01 (First Intermediate Folding Stage) to *Fs*=08 (Final Stage) by Structural Lighting Method	193
Figure 4.9	Raw 3-D Triangulation Mesh for Origami Model B05 (Degree-4 Vertices Inflated into Four Degree-3 Vertices) folded from *Fs*=01 (First Intermediate Folding Stage) to *Fs*=09 (Final Stage) by Structural Lighting Method	194
Figure 4.10	Raw 3-D Triangulation Mesh for Origami Model C10 (Four Elliptical Mountain Ridge Curves in Square) folded from *Fs*=01 (First Intermediate Folding Stage) to *Fs*=13 (Final Stage) by Structural Lighting Method	195
Figure 4.11	Raw 3-D Triangulation Mesh for Origami Model D13 (4-Lobed Cloverleaf Design) folded from *Fs*=01 (First Intermediate Folding Stage) to *Fs*=13 (Final Stage) by Structural Lighting Method	196
Figure 4.12	Outline Generation for Origami Model A03 (Four Degree-4 Vertices) folded from *Fs*=01 (First Intermediate Folding Stage) to *Fs*=08 (Final Stage) by Structural Lighting Method	198
Figure 4.13	Outline Generation for Origami Model B05 (Degree-4 Vertices Inflated into Four Degree-3 Vertices) folded from *Fs*=01 (First Intermediate Folding Stage) to *Fs*=09 (Final Stage) by Structural Lighting Method	199
Figure 4.14	Outline Generation for Origami Model C10 (Four Elliptical Mountain Ridge Curves in Square) folded from *Fs*=01 (First Intermediate Folding Stage) to *Fs*=13 (Final Stage) by Structural Lighting Method	200
Figure 4.15	Outline Generation for Origami Model D13 (4-Lobed Cloverleaf Design) folded from *Fs*=01 (First Intermediate Folding Stage) to *Fs*=13 (Final Stage) by Structural Lighting Method	201
Figure 4.16	Sub-surface Division for Origami Model A03 (Four Degree-4 Vertices) folded from *Fs*=01 (First Intermediate Folding Stage) to *Fs*=08 (Final Stage) by Structural Lighting Method	203
Figure 4.17	Sub-surface Division for Origami Model B05 (Degree-4 Vertices Inflated into Four Degree-3 Vertices) folded from *Fs*=01 (First Intermediate Folding Stage) to *Fs*=09 (Final Stage) by Structural Lighting Method	204
Figure 4.18	Sub-surface Division for Origami Model C10 (Four Elliptical Mountain Ridge Curves in Square) folded from	205

	Fs=01 (First Intermediate Folding Stage) to *Fs*=13 (Final Stage) by Structural Lighting Method	
Figure 4.19	Sub-surface Division for Origami Model D13 (4-Lobed Cloverleaf Design) folded from *Fs*=01 (First Intermediate Folding Stage) to *Fs*=13 (Final Stage) by Structural Lighting Method	206
Figure 4.20	Surface Mesh Generation for Origami Model A03 (Four Degree-4 Vertices) folded from *Fs*=00 (Un-fold Stage) to *Fs*=08 (Final Stage) by Structural Lighting Method	208
Figure 4.21	Surface Mesh Generation for Origami Model B05 (Degree-4 Vertices Inflated into Four Degree-3 Vertices) folded from *Fs*=01 (First Intermediate Folding Stage) to *Fs*=09 (Final Stage) by Structural Lighting Method	209
Figure 4.22	Surface Mesh Generation for Origami Model C10 (Four Elliptical Mountain Ridge Curves in Square) folded from *Fs*=01 (First Intermediate Folding Stage) to *Fs*=13 (Final Stage) by Structural Lighting Method	210
Figure 4.23	Surface Mesh Generation for Origami Model D13 (4-Lobed Cloverleaf Design) folded from *Fs*=01 (First Intermediate Folding Stage) to *Fs*=13 (Final Stage) by Structural Lighting Method	211
Figure 4.24	Comparison of Final Results of 3-D Surface Geometry Output Generated by Between ICM and SLM for All Origami Models during F_S=01	213
Figure 4.25	Illustration for Basis of Folding Process in Origami	214
Figure 4.26	Guiding Views from respective axis in describing the folding process for Origami Model A01	216
Figure 4.27	Top view (*X*-*Y* plane) of Model A01 (Square Degree-4 vertices of circle) from the start of folding stage 01 to the final folding stage 04	217
Figure 4.28	Front view (*X*-*Z* plane) of Model A01 (Square Degree-4 vertices of circle) from the start of folding stage 01 to the final fold stage 04	218
Figure 4.29	Side view (*X*+45°-*Z* plane) of Model A01 (Square Degree-4 vertices of circle) from the start of folding stage 01 to the final folding stage 04	219
Figure 4.30	Isometric view (3-Dimension) of Model A01 (Square Degree-4 vertices of circle) from the start folding stage 01 to the final folding stage 04	220

Figure 4.31	Outlines of Origami Model A01 (in Plan View) during the Folding Process from the Un-fold Stage 00 (Maroon Colour) to the Final Folding Stage 04 (Green Colour)	221
Figure 4.32	Outlines of Origami Model A01 (in Front View) during the Folding Process from the Un-fold Stage 00 (Maroon Colour) to the Final Folding Stage 04 (Green Colour)	222
Figure 4.33	Outlines of Origami Model A01 (in Plan View) during Folding Process	223
Figure 4.34	Outlines of Origami Model A01 (in Front View) during Folding Process in Changing Overall Height at the Center of Origami Model	223
Figure 4.35	Change in Angle of Rotation at Center (θ_C) during Folding Process for Origami Model A01	224
Figure 4.36	Change in Maximum Height at Center (H_C) for Origami Model A01	225
Figure 4.37	Outlines of Boundary for Origami Model A01 (in Plan View) during the Folding Process from the Un-Fold Stage 00 (Maroon Colour) to the Final Folding Stage 04 (Green colour)	225
Figure 4.38	Outlines of Boundary for Origami Model A01 (in Front View) during the Folding Process from the Un-Fold Stage 00 (Maroon Colour) to the Final Folding Stage 04 (Green colour)	226
Figure 4.39	Measurement of Image Pixel for Plan Area (A_C) during Folding Process for Origami Model A01	227
Figure 4.40	Pixel Measurement for the Change in Plan Area during Folding Process of Origami Model A01	228
Figure 4.41	Change in Plan Area (A_C) during Folding Process for Origami Model A01	229
Figure 4.42	Outlines of Valley Folds for Origami Model A01 (in Plan View) during the Folding Process from the Un-fold Stage 00 (Maroon Colour) to the Final Folding Stage 04 (Green Colour)	230
Figure 4.43	Outlines of Valley Folds for Origami Model A01 (in Front View) during the Folding Process from the Un-fold Stage 00 (Maroon Colour) to the Final Folding Stage 04 (Green Colour)	230
Figure 4.44	Outlines of Mountain for Origami Model A01 (in Plan View) during the Folding Process from the Un-fold Stage	231

	00 (Maroon Colour) to the Final Folding Stage 04 (Green Colour)	
Figure 4.45	Outlines of Mountain for Origami Model A01 (in Front View) during the Folding Process from the Un-fold Stage 00 (Maroon Colour) to the Final Folding Stage 04 (Green Colour)	231
Figure 4.46	Origami Model A01 (in Top View, *X*-*Y* plane) showing Measurement for Length of Mountain Folds from Center and Angular Measurement for Mountain Fold during Folding Process	233
Figure 4.47	Change in Length from Centre to the End of Mountain Fold for Origami Model A01	234
Figure 4.48	Change in Angle of Rotation of Mountain Fold during Folding Process for Origami Model A01	235
Figure 4.49	Measurement for Change in Height of Mountain Fold Lines at Boundaries during Folding Process for Origami Model A01: (a) Front view (*X*+45°-*Z*); and (b) Side view (Y+45°-Z)	236
Figure 4.50	Change in Height of Mountain Fold at Boundary during Folding Process for Origami Model A01	237
Figure 4.51	Illustrations of Geometrical Changes with respect to each Major Parametric Measurement for Origami Models under Category A during Folding Process	241
Figure 4.52	Graphs of Results for the Major Parametric Measurements for Origami Models under Category A	242
Figure 4.53	Guiding Views from respective axes in describing the folding process for Origami Model B04	244
Figure 4.54	Top View (*X*-*Y* plane) of Model B04 (Degree-4 Vertices Inflated into Two Degree-3 Vertices) from Fold Stage 01 to the Final Fold Stage 09	245
Figure 4.55	Front View (*X*-*Z* plane) of Model B04 (Degree-4 Vertices Inflated into Two Degree-3 Vertices) from Fold Stage 01 to the Final Fold Stage 09	246
Figure 4.56	Side View (*X*+45°-*Z* plane) of Model B04 (Degree-4 Vertices Inflated into Two Degree-3 Vertices) from Fold Stage 01 to the Final Fold Stage 09	247

Figure 4.57	Isometric View (3-D View) of Model B04 (Degree-4 Vertices Inflated into Two Degree-3 Vertices) from Fold Stage 01 to the Final Fold Stage 09	248
Figure 4.58	Outlines of Model B04 (in Plan View) during the Folding Process from the Un-fold Stage 00 (Maroon colour) to the Final Folding Stage 09 (Dark-blue Colour)	249
Figure 4.59	Outlines of Model B04 (in Front View, *X-Z* plane) during the Folding Process from the Un-fold Stage 00 (Maroon colour) to the Final Fold Stage 09 (Dark-blue Colour)	250
Figure 4.60	Outlines of Model B04 (in Side View, *Y-Z* plane) during the Folding Process from the Un-fold Stage 00 (Maroon colour) to the Final Fold Stage 09 (Dark-blue Colour)	251
Figure 4.61	Outlines of Model B04 (in plan view) during Folding Process showing change in angle of rotation at the Center	252
Figure 4.62	Outlines of Model B04 (in front view) during folding process showing the change in overall height at the center	252
Figure 4.63	Change in Angle of Rotation at Center (θ_C) during Folding Process for Origami Model B04	253
Figure 4.64	Change in Maximum Height at Center (H_C) during Folding Process for Origami Model B04	253
Figure 4.65	Outlines of Origami Boundary for Model B04 (in Plan View) during the Folding Process from the Un-fold Stage 00 (Maroon colour) to the Final Fold Stage 08 (Dark-blue Colour)	254
Figure 4.66	Outlines of Origami Boundary for Model B04 (in Front View) during the Folding Process from the Un-fold Stage 00 (Maroon colour) to the Final Fold Stage 08 (Dark-blue Colour)	255
Figure 4.67	Pixel Measurement for the Change of Plan Area of Origami Model B04	256
Figure 4.68	Change in Plan Area (AC) during Folding Process for Origami Model B04	257
Figure 4.69	Outlines of Valley-folds for Model B04 (in Plan View) during Folding Process from the Un-fold Stage 00 (Maroon colour) to the Final Fold Stage 09 (Dark-blue Colour)	258
Figure 4.70	Outlines of Valley-folds for Model B04 (in Front View, *X-Z* plane) during Folding Process from the Un-fold Stage 00	258

(Maroon colour) to the Final Fold Stage 09 (Dark-blue Colour)

Figure 4.71	Outlines of Valley-folds for Model B04 (in Side View, *Y-Z* plane) during Folding Process from the Un-fold Stage 00 (Maroon colour) to the Final Fold Stage 09 (Dark-blue Colour)	259
Figure 4.72	Outlines of Mountain-folds for Model B04 (in Plan View) during Folding Process from the Un-fold Stage 00 (Maroon colour) to the Final Folding Stage 09 (Dark-blue Colour)	259
Figure 4.73	Outlines of Mountain-folds for Model B04 (in Front View, *X-Z* plane) during Folding Process from the Un-fold Stage 00 (Maroon colour) to the Final Folding Stage 09 (Dark-blue Colour)	260
Figure 4.74	Outlines of Valley-folds for Model B04 (in Side View, *Y-Z* plane) during Folding Process from the Un-fold Stage 00 (Maroon colour) to the Final Fold Stage 09 (Dark-blue Colour)	261
Figure 4.75	Schematic Top View (*X-Y* Plane) of Origami Model B04 showing Measurement for Length between Edge of Mountain Folds and Angular Measurement for Mountain Fold during Folding Process	262
Figure 4.76	Changes in Angle of Rotation of Mountain Fold during folding process for Origami Model B04	263
Figure 4.77	Changes in Length between Two Mountain Folds during Folding Process for Origami Model B04	263
Figure 4.78	Schematic Side View (*X*+45°-*Z* Plane) of Origami Model B04 showing Measurement of Height of Mountain Fold at Boundary (H_{MB}) and the Height of Mountain Fold at Offset Point from the Center (H_{MC})	264
Figure 4.79	Change in Height of Mountain Fold at Boundary (H_{MB}) during Folding Process for Origami Model B04	265
Figure 4.80	Change in Height of Mountain Fold at Intersection Point Offset ffrom the Center (H_{MC}) for Origami Model B04	265
Figure 4.81	Illustrations of Geometrical Changes with respect to each Major Parametric Measurement for Origami Models under Category B during Folding Process	269
Figure 4.82	Graphs of Results for the Major Parametric Measurements for Origami Models under Category B	270

Figure 4.83	Guiding Views from respective axes in describing the folding process for Origami Model C08	272
Figure 4.84	Top View (*X*-*Y* plane) of Model C08 (Two Mountain Ridge Curves in Square) from Fold Stage 01 to the Final Fold Stage 09	273
Figure 4.85	Front View (*X*-*Z* plane) of Model C08 (Two Mountain Ridge Curves in Square) from Fold Stage 01 to the Final Fold Stage 09	274
Figure 4.86	Side View (*X*+45°-*Z* plane) of Model C08 (Two Mountain Ridge Curves in Square) from Fold Stage 01 to the Final Fold Stage 09	275
Figure 4.87	Side View (*Y*-*Z* plane) of Model C08 (Two Mountain Ridge Curves in Square) from Fold Stage 01 to the Final Fold Stage 09	276
Figure 4.88	Isometric View (3-D View) of Model C08 (Two Mountain Ridge Curves in Square) from Fold Stage 01 to the Final Fold Stage 09	277
Figure 4.89	Outlines of Origami Model C08 (in Plan View) during the Folding Process from the Un-fold Stage 00 (Maroon colour) to the Final Folding Stage 09 (Dark-blue Colour)	278
Figure 4.90	Outlines of Origami Model C08 (in Front View, *X*-*Z* plane) during the Folding Process from the Un-fold Stage 00 (Maroon colour) to the Final Folding Stage 09 (Dark-blue Colour)	279
Figure 4.91	Outlines of Origami Model C08 (in Side View, *Y*-*Z* plane) during the Folding Process from the Un-fold Stage 00 (Maroon colour) to the Final Folding Stage 09 (Dark-blue Colour)	279
Figure 4.92	Outlines of Origami Model C08 (in Plan View) during Folding Process	280
Figure 4.93	Outlines of Origami Model C08 (in Front View) during Folding Process Folding Process in Changing Overall Height at the Center of Origami Model	280
Figure 4.94	Change in Maximum Height at Center (H_C) during Folding Process for Origami Model C08	281
Figure 4.95	Outlines of Origami Boundary for Origami Model C08 (in Plan View) during the Folding Process from the Un-fold Stage 00 (Maroon colour) to the Final Folding Stage 09 (Dark-blue Colour)	282

Figure 4.96	Outlines of Origami Boundary for Origami Model C08 (in Side View, *X*-*Z* plane) during the Folding Process from the Un-fold Stage 00 (Maroon colour) to the Final Folding Stage 09 (Dark-blue Colour)	283
Figure 4.97	Outlines of Origami Boundary for Origami Model C08 (in Side View, *X*-*Z* plane) during the Folding Process from the Un-fold Stage 00 (Maroon colour) to the Final Folding Stage 09 (Dark-blue Colour)	283
Figure 4.98	Outlines of Boundary (in Side View) showing Measurement of Maximum Height at boundary (H_B) during Folding Process of Origami Model C08	284
Figure 4.99	Change in Maximum Height at Boundary (H_B) during Folding Process for Model C08	284
Figure 4.100	Pixel Measurement for the Change of Plan Area (A_C) during Folding Process for Origami Model C08	285
Figure 4.101	Change in Plan Area (A_C) during Folding Process for Model C08	286
Figure 4.102	Outlines of Mountain Folds for Origami Model C08 (in Plan View) during the Folding Process from the Un-fold Stage 00 (Maroon colour) to the Final Folding Stage 09 (Dark-blue Colour)	287
Figure 4.103	Outlines of Mountain Folds for Origami Model C08 (in Front View, *X*-*Z* plane) during the Folding Process from the Un-fold Stage 00 (Maroon colour) to the Final Fold Stage 09 (Dark-blue Colour)	287
Figure 4.104	Outlines of Mountain Folds for Origami Model C08 (in Side View, *Y*-*Z* plane) during the Folding Process from the Un-fold Stage 00 (Maroon colour) to the Final Fold Stage 09 (Dark-blue Colour)	288
Figure 4.105	Origami Model C08 (in Top View, *X*-*Y* plane) showing Measurement for Length between Edge of Mountain Folds during Folding Process	288
Figure 4.106	Change in Length between two Mountain Folds (ℓ_{MF}) during Folding Process for Model C08	289
Figure 4.107	Origami Model C08 (in Side View, *X*-*Y* plane) showing the Measurement of Maximum Height of Mountain Folds (H_{MC})	289
Figure 4.108	Change in Height of Mountain Fold at Center (H_{MC}) during Folding Process for Origami Model C08	290

Figure 4.109	Illustrations of Geometrical Changes with respect to each Major Parametric Measurement for Origami Models under Category C during Folding Process	294
Figure 4.110	Graphs of Results for the Major Parametric Measurements for Origami Models under Category C	295
Figure 4.111	Guiding Views from respective axes in describing the folding process for Origami Model D13	296
Figure 4.112	Top View (*X*-*Y* plan) of Solid Rendered Model M13 (4-Lobed Cloverleaf Design) from Fold Stage 01 to the Final Fold Stage 06	297
Figure 4.113	Front View (*X*-*Z* plan) of Solid Rendered Model M13 (4-Lobed Cloverleaf Design) from Fold Stage 01 to the Final Fold Stage 06	298
Figure 4.114	Side View (*X*+45°-*Z* plan) of Solid Rendered Model D13 (4-Lobed Cloverleaf Design) from Fold Stage 01 to the Final Fold Stage 06	299
Figure 4.115	Isometric View (3-D View) of Solid Rendered Model D13 (4-Lobed Cloverleaf Design) from Fold Stage 01 to the Final Fold Stage 06	300
Figure 4.116	Outlines of Origami Model D13 (in Plan View) during the Folding Process from the Un-fold Stage 00 (Maroon colour) to the Final Fold Stage 03 (Spring-green Colour)	301
Figure 4.117	Outlines of Origami Model D13 (in Front View) during the Folding Process from the Un-fold Stage 00 (Maroon colour) to the Final Fold Stage 03 (Spring-green Colour)	302
Figure 4.118	Outlines of Origami Model D13 (in Plan View) during Folding Process	303
Figure 4.119	Outlines of Origami Model D13 (in Front View) during Folding Process in Changing Overall Height at the Center of Origami Model	303
Figure 4.120	Changes in Height at Center (H_C) during Folding Process for Origami Model D13	304
Figure 4.121	Outlines of Boundary for Origami Model D13 (in Plan View) during the Folding Process from the Un-fold Stage 00 (Maroon colour) to the Final Folding Stage 06 (Spring-green Colour)	305
Figure 4.122	Outlines of Boundary for Origami Model D13 (in Front View) during showing the Folding Process from the Un-	305

fold Stage 00 (Maroon colour) to the Final Folding Stage 06 (Spring-green Colour)

Figure 4.123 Outlines of Origami Model D13 (in Top View) showing Measurement of Changes in Diagonal Length of Boundary (ℓ_d) during Folding Process 306

Figure 4.124 Change in Length of Diagonal (ℓ_d) during Folding Process for Origami Model D13 306

Figure 4.125 Outlines of Boundary (in Side View) showing Measurement of Maximum Height at boundary (H_B) during Folding Process of Origami Model D13 307

Figure 4.126 Change in Maximum Height at Boundary (H_B) during Folding Process for Model D13 307

Figure 4.127 Pixel Measurement for the Change of Plan Area (A_C) during Folding Process for Origami Model C13 308

Figure 4.128 Change in Plan Area (A_C) during Folding Process for Origami Model D13 309

Figure 4.129 Outlines of All Folding Lines for Origami Model D13 (in Plan View) during the Folding Process from the Un-fold Stage 00 (Maroon colour) to the Final Fold Stage 06 (Spring-green Colour) 310

Figure 4.130 Outlines of All Folding Lines for Origami Model D13 (in Front View) during the Folding Process from the Un-fold Stage 00 (Maroon colour) to the Final Fold Stage 06 (Spring-green Colour) 310

Figure 4.131 Outlines of Origami Model D13 (in front view) showing the Measurement of Maximum Height of Valley Folds (H_{VC}) during Folding Process 311

Figure 4.132 Change in Height of Valley Folds at Center (H_{VC}) during Folding Process for Origami Model D13 311

Figure 4.133 Illustrations of Geometrical Changes with respect to each Major Parametric Measurement for Origami Models under Category D during Folding Process 315

Figure 4.134 Graphs of Results for the Major Parametric Measurements for Origami Models under Category D 316

Figure 4.135 Stress Resultant and Sign Convention acting on Quadrilateral Thin Shell Surface Element 321

Figure 4.136 Contour Diagram of Stress Resultant in Local x Direction (N_x) for Model C11 with Different Surface Geometry: (a) 332

Fs=01 (Start of Folding Stage); (b) *Fs*=02 and; (c) *Fs*=03 (End of Folding Stage)

Figure 4.137 Contour Diagram of Stress Resultant in Local *y* Direction (N_y) for Model C11 with Different Surface Geometry: (a) *Fs*=01 (Start of Folding Stage); (b) *Fs*=02 and; (c) *Fs*=03 (End of Folding Stage) 333

Figure 4.138 Contour Diagram of Stress Resultant in Local *xy* Plane (N_{xy}) for Model C11 with Different Surface Geometry: (a) *Fs*=01 (Start of Folding Stage); (b) *Fs*=02 and; (c) *Fs*=03 (End of Folding Stage) 334

Figure 4.139 Contour Diagram of Stress Resultant in Local *x* Direction (N_x) for Model D13 with Different Surface Geometry: (a) *Fs*=01 (Start of Folding Stage); (b) *Fs*=02; (c) *Fs*=03; (d) *Fs*=04; (e) *Fs*=05 and; (f) *Fs*=06 (End of Folding Stage) 335

Figure 4.140 Contour Diagram of Stress Resultant in Local *y* Direction (N_y) for Model D13 with Different Surface Geometry: (a) *Fs*=01 (Start of Folding Stage); (b) Fs=02; (c) Fs=03; (d) *Fs*=04; (e) *Fs*=05 and; (f) *Fs*=06 (End Folding Stage) 336

Figure 4.141 Contour Diagram of Stress Resultant in Local xy Plane (N_{xy}) for Model D13 with Different Surface Geometry: (a) *Fs*=01 (Start of Folding Stage); (b) *Fs*=02; (c) *Fs*=03; (d) *Fs*=04; (e) *Fs*=05 and; (f) *Fs*=06 (End of Folding Stage) 337

Figure 4.142 Moment Resultant and Sign Convention acting on Quadrilateral Thin Shell Surface Element 340

Figure 4.143 Moment Resultant over Shell Middle-Surface 348

Figure 4.144 Contour Diagram of Moment Resultant in Local *x* Direction (M_x) for Model C11 with Different Surface Geometry: (a) *Fs*=01 (Start of Folding Stage); (b) *Fs*=02 and; (c) *Fs*=03 (End of Folding Stage) 351

Figure 4.145 Contour Diagram of Moment Resultant in Local *y* Direction (M_y) for Model C11 with Different Surface Geometry: (a) *Fs*=01 (Start of Folding Stage); (b) *Fs*=02 and; (c) *Fs*=03 (End of Folding Stage) 352

Figure 4.146 Contour Diagram of Moment Resultant in Local *xy* Plane (M_{xy}) for Model C11 with Different Surface Geometry: (a) *Fs*=01 (Start of Folding Stage); (b) *Fs*=02 and; (c) *Fs*=03 (End of Folding Stage) 353

Figure 4.147 Contour Diagram of Moment Resultant in Local *x* Direction (M_x) for Model D13 with Different Surface Geometry: (a) 354

Fs=01 (Start of Folding Stage); (b) *Fs*=02; (c) *Fs*=03; (d) *Fs*=04; (e) *Fs*=05 and; (f) *Fs*=06 (End of Folding Stage)

Figure 4.148 Contour Diagram of Moment Resultant in Local *y* Direction (M_y) for Model D13 with Different Surface Geometry: (a) *Fs*=01 (Start of Folding Stage); (b) *Fs*=02; (c) *Fs*=03; (d) *Fs*=04; (e) *Fs*=05 and; (f) *Fs*=06 (End of Folding Stage) 355

Figure 4.149 Contour Diagram of Moment Resultant in Local *xy* Plane (M_{xy}) for Model D13 with Different Surface Geometry: (a) *Fs*=01 (Start of Folding Stage); (b) *Fs*=02; (c) *Fs*=03; (d) *Fs*=04; (e) *Fs*=05 and; (f) *Fs*=06 (End of Folding Stage) 356

Figure 4.150 Appearance of Geometrical shapes for Origami Models under Category C and D with Similarity as Dome Surface Structure 358

Figure 4.151 Maximum Resultant Displacement (RSLT) of SSCFL with geometry corresponding to different folding stage of Model C11 361

Figure 4.152 Displacement Contour Diagrams for SSCFL (Model C11) with Different Surface Geometry: (a) *Fs*=01 (Start of Folding Stage); (b) *Fs*=02 and; (c) *Fs*=03 (End of Folding Stage) 363

Figure 4.153 Sectional Cut between Two-supports (*A-A'*) of SSCFL (Model C11) 364

Figure 4.154 Resultant Displacement for the Cutting Section between Two-supports for SSCFL (Model C11) 364

Figure 4.155 Sectional Cut between Two Non-supporting Points (*B-B'*) of SSCFL (Model C11) 365

Figure 4.156 Resultant Displacement for the Cutting Section between Two Non-supporting Points for SSCFL (Model C11) 365

Figure 4.157 Maximum Resultant Displacement (RSLT) with respects to the Stage of Folding for SSCFL (Model C12) 366

Figure 4.158 Displacement Contour Diagrams for SSCFL Model C12 with Different Surface Geometry: (a) *Fs*=01 (Start of Folding Stage); (b) *Fs*=02 and; (c) *Fs*=03; (d) *Fs*=04; (e) *Fs*=05 and; (f) *Fs*=06 (End of Folding Stage) 368

Figure 4.159 Sectional Cut between Two-supports (*A-A'*) of SSCFL (Model C12) 369

Figure 4.160 Resultant Displacement for the Cutting Section between Two-supports for SSCFL (Model C12) 369

Figure 4.161 Sectional Cut between Two Non-supporting Points (*B-B'*) of SSCFL (Model C12) 370

Figure 4.162 Resultant Displacement for the Cutting Section between Two Non-supporting Points for SSCFL (Model C12) 370

Figure 4.163 Maximum Resultant Displacement (RSLT) in SSCFL (Model D13) models 371

Figure 4.164 Displacement Contour Diagrams for SSCFL (Model D13) with Different Surface Geometry: (a) *Fs*=01 (Start of Folding Stage); (b) *Fs*=02 and; (c) *Fs*=03; (d) *Fs*=04; (e) *Fs*=05 and; (f) *Fs*=06 (End of Folding Stage) 373

Figure 4.165 Sectional Cut between Two-supports (*A-A'*) of SSCFL (Model D13) 374

Figure 4.166 Resultant Displacement for the Cutting Section between Two-supports for SSCFL (Model D13) 374

Figure 4.167 Sectional Cut between Two Non-supporting Points (*B-B'*) of SSCFL (Model D13) 375

Figure 4.168 Resultant Displacement for the Cutting Section between Two Non-supporting Points for SSCFL (Model D13) 375

LIST OF ABBREVIATIONS

CAD	Computer-aid design
DAVID SLS-1	DAVID Structured Lighted System version 1
DLG	Double layer grid
DWG	Drawing format file for storing 2-D to 3-D design data
DXF	Drawing exchange format for CAD based system
ESPI	Electronic speckle pattern interferometry
FEM	Finite element modeling
ICM	Image capturing method
LUSAS	A finite element analysis application software
MESHLAB	Advanced 3-D mesh processing software system
NURB	Non-uniform rational B-spline
OBJ	Object file format for definition of 3-D geometry
QSL8	Quadrilateral semiloof curved thin shell element
RE	Reverse engineering
RSLT	Resultant
SLG	Single layer grid
SLM	Structured light method
SPLINE	Special function of line defined piecewise by polynomials
SSCFL	Shell structure with curved fold lines

LIST OF SYMBOLS

A_C	Percentage area of coverage within the boundary lines of origami model
C_S	Camera positioned at side from object for image capturing
C_T	Camera positioned at top from object for image capturing
f_c	Characteristic compressive strength
F_d	Folding distance
${}^{f}Fs$	Final folding stage
${}^{fi}Fs$	First intermediate folding stage
F_S	Folding stage
f_s	Shear strength capacity
f_t	Tensile strength capacity
Gn	Numbering sequence for grid lines
H_B	Maximum height measured at boundary of origami model
H_C	Maximum height measured at center of origami model
H_M	Maximum height measured at mountain fold line of origami model
H_{MB}	Height of mountain fold at boundary
H_{MC}	Height of mountain fold at the center
H_V	Maximum height measured at valley fold line of origami model
H_{VC}	Height of valley fold at center
${}^{i}Fs$	Intermediate folding stage
l	Length between two supports of origami model
ℓ_B	Maximum length measured between boundary lines of origami model
ℓ_M	Maximum length measured between ends of mountain fold lines of origami model

ℓ_{MF}	Length from center to the end of mountain fold
ℓ_V	Maximum length measured between ends of valley fold lines of origami model
M_{all}	Allowable moment resultant
MF	Mountain fold
M_x	Moment resultant per unit width of thin shell element in local Cartesian system of x direction
M_{xy}	Twisting moment resultant per unit width of thin shell element in local Cartesian system of xy plane
M_y	Moment resultant per unit width of thin shell element in local Cartesian system of x direction
N_{all}	Allowable stress resultant
N_x	Stress resultant per unit width of thin shell element in local Cartesian system of x direction
N_{xy}	Stress resultant per unit width of thin shell element in local Cartesian system of xy plane
N_y	Stress resultant per unit width of thin shell element in local Cartesian system of y direction
O_S	Optical projector positioned at side from object for scanning
O_T	Optical projector positioned at top from object for scanning
T	Thickness of shell surface
VF	Valley fold
θ_B	Angle of rotation measured between ends of boundary lines with respect to original alignment
θ_C	Angle of rotation measured at center of origami model with respect to original alignment
θ_M	Angle of rotation measured between ends of mountain fold lines with respect to original alignment
θ_V	Angle of rotation measured between ends of valley fold lines with respect to original alignment
σ	Nominal stress
σ_{all}	Allowable stress

STRUKTUR LIPAT BERASASKAN KONSEP ORIGAMI DENGAN GARIS LIPAT MELENGKUNG

ABSTRAK

Origami dengan garis lipat melengkung mempunyai ciri-ciri permukaan melengkung yang dirangkumi oleh garis lipat melengkung yang boleh digunakan secara bermanfaat sebagai struktur lipat. Walau bagaimanapun, potensi penggunaan origami dengan garis lipat melengkung didapati tidak banyak dikaji kerana proses melipat yang kompleks dengan pelbagai susun atur dan konfigurasi garis lipat melengkung. Kajian ini dijalankan untuk menyiasat ciri-ciri proses lipatan origami dengan garis lipat melengkung. Kesan geometri permukaan origami dengan garis lipat melengkung pada peringkat lipatan yang berlainan ke atas tingkah-laku struktur kekerang dengan garis lipat melengkung (SSCFL) juga ditentukan. Satu set kriteria telah dibangunkan dalam mengklasifikasikan origami dengan garis lipat melengkung yang dicipta oleh ramai penyelidik atau ahli sains origami dan digunakan dalam klasifikasi 51 model origami kepada 11 kumpulan. Daripada 51 model, sejumlah 13 model origami yang berpotensi untuk digunakan sebagai struktur lipat telah dipilih dan dikumpulkan semula ke dalam empat kategori utama seperti berikut: *Non-inflated n Degree-n Vertices* (kategori A), *Inflated n Degree-n Vertices* (kategori B), *n Curve Mountain Ridge* (kategori C), dan Bentuk kompleks (kategori D). Perolehan data permukaan 3-D dengan teknik pengukuran imej tanpa sentuh seperti kaedah penangkapan imej dan kaedah cahaya berstruktur, digunakan untuk mendapatkan model geometri origami dengan lipatan melengkung yang tepat. Prosedur berasaskan CAD dalam penjanaan model geometri origami 3-D dengan garis lipat melengkung telah dibangunkan. Mekanisme lipatan berdasarkan penilaian ke atas set pengukuran atau parameter yang mewakili perubahan

geometri permukaan model origami semasa proses lipatan telah dikaji. Daripada hasil pengukuran, didapati proses lipatan origami di bawah kategori A dan B diiringi dengan ubahbentuk berputar terhadap pusat model. Tiada ubah bentuk berputar diperhatikan dalam proses lipatan origami di bawah kategori C dan D. Model di bawah kategori C (*n Curve Mountain Ridge*) khususnya C10 menunjukkan perubahan terbesar dalam ketinggian maksimum di pusat model, dan pengurangan terbesar dalam saiz pelan origami semasa proses lipatan. Sementara itu, perubahan geometri dari segi sudut putaran maksimum di pusat dan penjuru model origami didapati berlaku dalam Model B06 di bawah kategori B (*Inflated n Degree-n Vertices*). Perubahan maksimum ketinggian di sempadan didapati berlaku dalam Model B04. Satu siri model SSCFL dengan geometri permukaan model origami masing-masing di peringkat lipatan yang berbeza telah dihasilkan. SSCFL ini adalah 100 kali ganda saiz model origami masing-masing dengan ketebalan permukaan 200 mm (permukaan keseluruhan) dan 250 mm (di kawasan sokongan). SSCFL dikenakan sokongan garis dan dimodelkan menggunakan konkrit kekuatan normal. Keputusan analisis elemen terhad di bawah keadaan berat sendiri menunjukkan bahawa model SSCFL di bawah kategori C (khususnya geometri permukaan yang berkaitan dengan C11 dan C12) dan kategori D (D13) memenuhi had tegasan atas sebab kemiripannya dengan struktur kubah. Sebaliknya, model SSCFL di bawah kategori A dan B gagal memenuhi had tegasan kerana sifat geometri permukaan yang tidak simetri dan kewujudan sempadan struktur dengan panjang terjulur yang agak besar. Model SSCFL didapati menunjukkan prestasi yang cemerlang dari segi kekukuhan atas sebab wujudnya lipatan melengkung yang meningkatkan kedalaman efektif struktur yang berkesan.

FOLDABLE STRUCTURE BASED ON ORIGAMI WITH CURVED FOLD LINES CONCEPT

ABSTRACT

Origami with curved fold lines possesses characteristic feature of curved surface bounded by curved fold lines which can be advantageously adopted for foldable structures. However, potential use of origami with curved fold lines has not been much studied due to complexity of the folding process under many different possible layouts and configurations of curved fold lines. This study is carried out to investigate the characteristics of the folding process of origami with curved fold lines. Effect of surface geometry at different folding stage of origami with curved fold lines on structural behaviour of shell structure with curved fold lines (SSCFL) was also determined. A set of criteria in classifying origami with curved fold lines created by many researchers or origami scientist has been established and used in the classification of 51 origami models into 11 groups. From the 51 models, 13 number of origami models with potential application as foldable structures have been chosen and regrouped into the following four main categories: Non-inflated *n* Degree-*n* Vertices (category A), Inflated *n* Degree-*n* Vertices (category B), *n* Mountain Ridge Curve (category C), and the Complex Shape (category D). 3-D surface data acquisition using optical non-contact measuring techniques of image capturing method and structured light method were used to obtain an accurate geometrical model of origami with curved folds. CAD based procedures in generating 3-D geometrical model of origami with curved fold lines have been developed. The folding mechanism based on the evaluation of a set of measurement or parameter representing change in surface geometry of the origami models during the folding process has been studied. From the results of

measurements, it is found that folding process of origami under categories A and B is accompanied by twisting deformation about the center of the model. No twisting deformation is observed in folding process of origami under categories C and D. Models under category C (*n* Mountain Ridge Curve) specifically C10 shows the largest change in maximum height at center of model, and largest reduction in plan area of origami during folding process. Meanwhile, change in geometry in term of maximum angle of rotation of the center and boundary of origami model is found to occur in Model B06 under category B (Inflated *n* Degree-*n* Vertices). The maximum change in height at boundary is found to occur in Model B04. A series of SSCFL models with surface geometry of the respective origami model at different folding stage have been generated. These SSCFL are 100 times scaled up models of respective origami model with surface thickness of 200 mm (overall surface) and 250 mm (at support regions). The SSCFL were assigned with line supports and modelled using normal strength concrete. Results of finite element analysis under self-weight show that SSCFL models under category C (specifically surface geometry associated with C11 and C12) and category D (D13) satisfy stress limit due to their resemblance to dome structure. On the other hand, SSCFL models under categories A and B failed to satisfy stress limit due to unsymmetrical nature of the surface geometry and existence of free boundary of structure with relatively large overhang length. SSCFL models were found to exhibit superior performance in terms of stiffness due to existence of curved folds which increases the effective depth of the structure.

CHAPTER ONE

INTRODUCTION

1.1 General

Nowadays, most large span roof structural systems are concerned not only the protection from weather effect but also economy by minimizing costs within the constraints of functional and aesthetic requirements. Designers thus try to search new forms such as shell and folded plate structures that can resist loads more efficiently than when the structure is designed in conventional form using slab and beam. For covering a given area by a roof, conventionally, as column spacing becomes larger, the sizes of beams increase, thereby making the structure uneconomical and aesthetically unpleasing. Alternatively, to cover the same area, a curved surface or folded surface can be conceived that carries the loads mainly in direct tension or compression, rather than in bending and shear as in the case of slab and beam structures. Even with a relative small thickness, shell and folded plate structures can sustain more loads over large column-free areas with a minimum deflection.

Over the last few decades, advancements in the structural analysis domain and computational tools enable engineers to satisfactorily analyze and build folded shells not just in various types and forms, but also as a foldable surface structure by folding or retracting the surface to transform size or dimension upon necessity of functions of venue requirement. Foldability of surface structures with wide variety of shapes and breathtaking elegance can be seen in origami. The available of advancement in technology nowadays allows design and construction of long spanning roof structural system infused with surface geometry inspired by the concept of origami. Furthermore, the kinematic characteristic of origami allows a flat piece of paper to transform from initial 2-D flat surface (open-stage) into 3-D geometry (closed-stage) via the process of folding. Thence, the uniqueness of origami with the properties of thin folding paper (equivalent to folded plate structure) and geometrical transform during folding process (equivalent to foldable structures) could be adopted as a new design for large spanning roof structure.

1.2 Background of Study

Long span roof surface structures are generally constructed with column-free internal space with span between supports of more than 12 meters in length (Chang and Swenson, 2017, Lisantono and Arfiadi, 2013, Roof, 2017, Beams, 2017, Munch - Andersen and Dietsch, 2011). High tensile strength materials which are thin and light are typically the choice in fabricating this structural system, making it flexible in term of geometry changes and during process of erection and dismantle, which subsequently reduce sub-structural costs and construction time. Examples of large span structural system commonly found in wide range of application are stadia, gymnasiums, arenas, factories, warehouses, malls, agricultural buildings, and coverage for swimming polls. The structural system are typically classified into five major groups of structural forms: space structures, cable structures, membrane structures, hybrid structures and convertible roofs (Majowiecki, 2005) as illustrated in Figure 1.1.

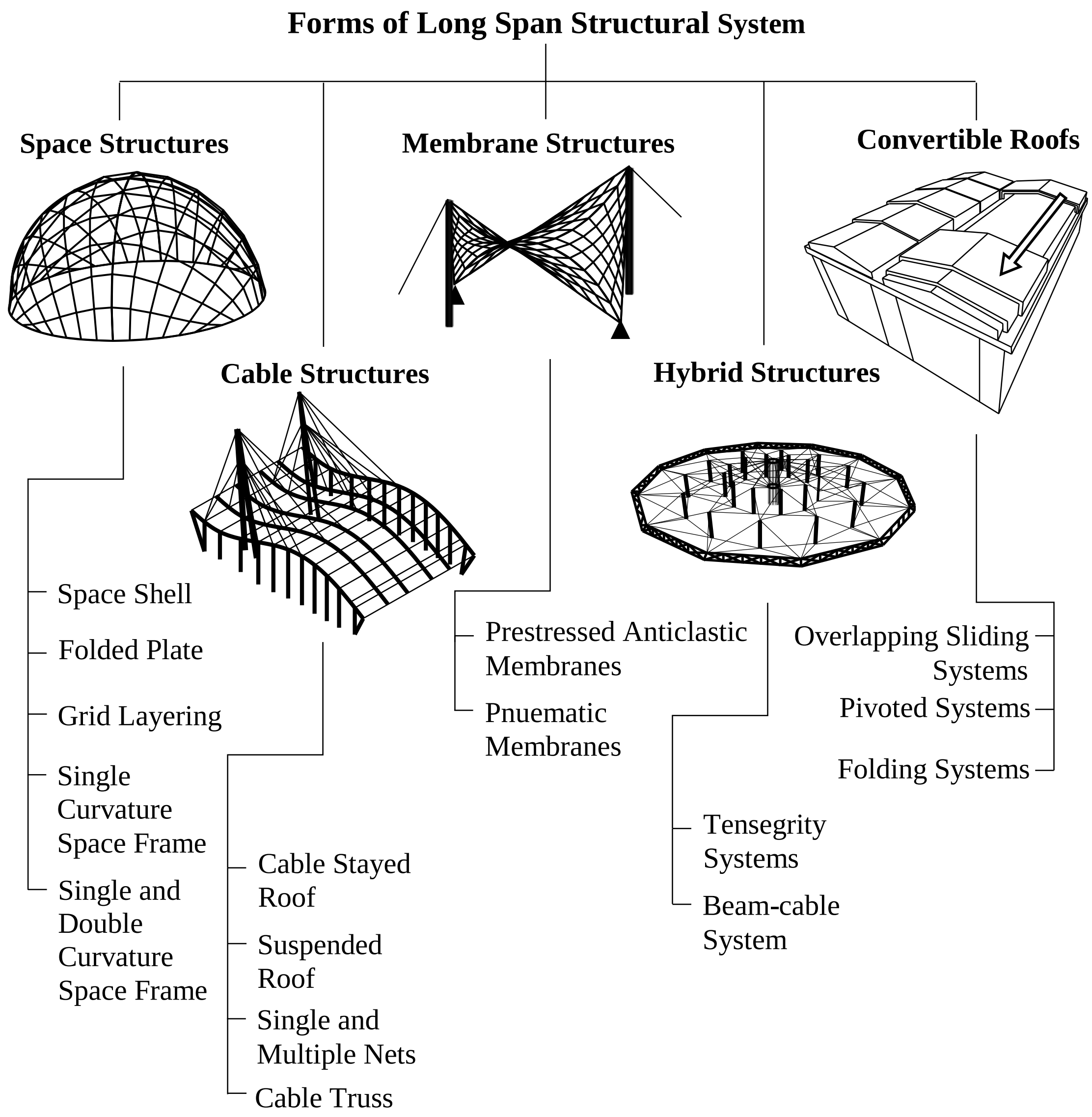

Figure 1.1- Typologies for the Forms of Long Span Roof Structural System

Space structures normally refer to a space frame in the form of a truss-like, lightweight rigid structure constructed from interlocking struts in a geometrical pattern such as single or multilayers of grid structures. Dome space structure is one the typical example of structure form under this category. Figure 1.2(a) shows one of the two biggest wooden dome to cover the bunkers of the "Federico II" Enel power plant in Brindisi by Holzbau (2015). The dome building was built with clear span of 143 meters in diameter and 50 meters in total height. Besides, space shell and folded plate structures are constructed by assembling small units of shell in which its thickness is small compared to the other dimensions. This allows its surface to be built in curved geometry with either single curvature or multi curvature.

Secondly, cable structures are those where the main elements that support the load, such as wires, cables, chains, and nets, are subjected only to tensile forces. Typical example of cable structures are bridges and roofs in which its plane or horizontal structures are fastened to supports by a series of wires. Figure 1.2(b) shows the Penang Second Bridge in Malaysia built by using cable stayed structural system with longest span between supports of 240 meters length which completed in year 2014 (Yadollahi et al., 2015).

For third, membrane structures are one of the long span structural system that made out of tensioned membrane or fabric materials such as PTFE glass and PVC polyester which are extremely strong in tension. The structural use of the membrane is divided into prestressed anticlastic membrane and pneumatic membrane. A famous example of successful application of membrane structural system is Beijing National Aquatics Center or called as The Water Cube in Beijing, China for the use of Olympics 2008 as shown in Figure 1.2(c). The tension fabric used in the structure is ETFE membrane with 0.2 mm in total thickness (Edmondson, 2012).

Next, hybrid structures are another advanced structural system that combine use of an isolated components in compression inside a net of continuous tensile properties of cables, in such a way that the compressed members (usually bars or struts) do not touch each other and the prestressed tensioned members (usually cables or tendons) delineate the system spatially (Jáuregui, 2010). Typical example of the structural systems are tensegrity and beam-cable. La Plata Stadium (Figure 1.2(d)) in Buenos Aires, Argentina is one of the most successful hybrid roofing structure which opened in 2003 (Wiki, 2017).

Lastly, convertible roof or called foldable roof is another choice of roof structural system. It allows the roof surface to be retractable or foldable for transforming an indoor space into an outdoor environment. A folding mechanism is designed for the specific type of convertible structure. Figure 1.2(e) shows a multi-purpose retractable roof stadium of the Mercedes-Benz Stadium in Atlanta, Georgia which was just opened in August 2017. It is designed with 8 triangular rigid-translucent-panels retractable by sliding of pinwheel to create a folding mechanism for opening the roof centrifugally towards the outside perimeters of the roof structure (Mercedes-Benz, 2017).

(a) Geodesic Dome Structures in Brindisi, Italy

(b) Penang Second Bridge in Pulau Pinang, Malaysia

Figure 1.2- Successful Application of Long Span Structural System: (a) Space Structure (Holzbau, 2015); (b) Cable Structure (Fauzi, 2012); (c) Membrane Structure (Cube, 2016); (d) Hybrid Structure (Wiki, 2017); and (e) Convertible Structure (Mercedes-Benz, 2017)

(c) Water Cube (National Aquatics Center) in Beijing, China

(d) La Plata Stadium in Buenos Aires, Argentina

(e) Mercedes-Benz Stadium in Atlanta, Georgia

Figure 1.2- Continued

1.2.1 Roof Structures with Folded Shell System

With the combination of thin surface structure of shell elements and strength enhancement feature along with the folded system, a kind of roof structure system called the fold shell possess structural similarities with origami. There are many application of this kind of structural system which have successfully been built.

In the year 1955, Royan Central Market in Nouvelle-Aquitaine, France (Figure 1.3(a)) is constructed in the form of multi-layer conoidal shape extruded from the center of the structure which create folding effect along its perimeter of the hall (Janberg, 1998b). The span of the thin folded shell is in 52.4 m and height up to 10.5 m with just 8.0 cm of its thickness (Tourisme, 2015).

The corrugated concrete dome of State Farm Center (Figure 1.3(b)) is another application of the concept of long span folded shell structure. The shape of surface takes the form of branching triangular folds with a span of around 122.7 m (Janberg, 1998a). In the same year, TWA Flight Center at New York of USA (Figure 1.3(c)) was built with concrete shell (Jen, 2011).

Miami Marine Stadium in Florida, United States built in 1963 (Figure 1.3(d)) is a dedicated example of roof structural system design in the form of folded shell. The geometrical shape of a single panel is in the hyperbolic paraboloid cantilevering shell which folded at the center along the support. It was considered as one of the longest span of cantilevered concrete folded shell structure in the world at the time it was built (Candela, 2008, Adriaenssens et al., 2014).

In 1973, a double curvature thin shell structural building called the Sydney Opera House was constructed in Sydney, Australia (Figure 1.3(e)). Prestressed concrete material was used for the long span length of up to 183 m (Janberg, 2006).

Another multi-conoidal thin folded thin shell structural form that was built in 2013 is L'Oceanogràfic Marine Complex in Valencia, Spain (Figure 1.3(f)) which is the largest complex of its type in Europe with total surface coverage of up to 110,000 m^2. The length of span of shell between supports is 35.5 m with the shell thickness of just 6 cm (Janberg, 2007).

Lastly, the most recent long span roof structure that in the form system of folded shell is the Kauffman Center for the Performing Arts in Missouri, United States (Figure 1.3(g)). Design of the roof consists of two symmetrical half shells in vertical alignment. Repetitive of scaling down the circular half shell surface creates an folded effect of the entire roof system (Arts, 2017, contributors, 2017c).

(a) Royan Central Market in Nouvelle-Aquitaine, France (Tourisme, 2015)

(b) State Farm Center in Illinois, USA (Dori, 2003, Benkrut, 2013)

(c) Trans World Flight Center in New York, United State (Avdeev, 2015)

Figure 1.3- Some Applications of Folded Shell Structures

(d) Miami Marine Stadium in Florida, United States (Candela, 2008)

(e) Sydney Opera House in Bennelong Point, Sydney (Janberg, 2006)

(f) L'Oceanogràfic Marine Complex in Valencia, Spain (Janberg, 2007)

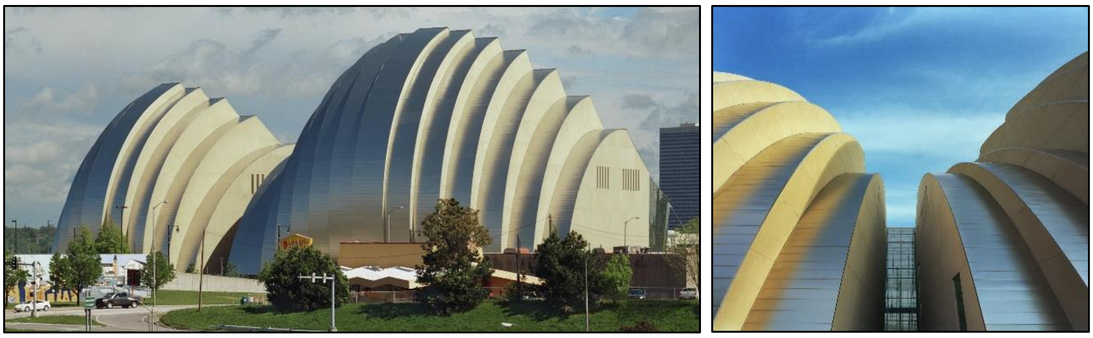

(g) Kauffman Center in Missouri, United States (Husley, 2011)

Figure 1.3- Continued

1.2.2 Roof Structures with Foldable Design

Foldable surface is one of the main characteristic of origami, with the capability to transforming from a flat surface (open-stage) to a 3-D geometry of retracted or stowed form (closed-stage). The foldable or retractable structures are also called as kinetic architectural structures.

Dated back to the year of 1961, Civic Arena (Figure 1.4(a)) was the first retractable roof major-sports venue in the world with coverage area of 15,794 m^2. The dome shaped roof was designed with eight individual panels. Six out of them are capable to retract by folding beneath adjacent panels along the perimeter of the dome (contributors, 2017a, Hockey, 1999).

For facilitating the international event of 1976 Summer Olympics in Canada, a stadium with retractable roof structure named the Montreal Olympic Stadium was constructed (Figure 1.4(b)). It was designed with a cantilever tower that could retract a series of cables holding the roof membrane for transforming it to indoor or outdoor field. The roof membrane retractable structure could cover area up to 5,500 m^2 (Baseball, 2001, contributors, 2017e, Janberg, 2003).

Umbrella-type structures are another example of pivotal folding system that retracts surface with centric configuration, such as the 17 m × 18 m large automatically controlled umbrellas proposed in 1992 by SL-Rasch GmbH (Rasch, 1980) for the courts of the Prophet's Holy Mosque in Madinah (Stevenson, 2011) as shown in Figure 1.4(c). Tension fabric material of PTFE membrane was used to form bell-shaped roof system when it is in open stage (MakMax, 2016, Soto, 2017).

In the year of 1999, Jaén Auditorium a retractable roof structure in Spain is constructed based on the principle of linkage bars and scissor system (Figure 1.4(d)). It is built with a series of steel arches that could folds by translating horizontally over a rail in which have the tensioned fabric between them to achieve a practical deployment process that fits together the structure and the enclosure while temporarily covers a specific area (Escrig, 1999, Torres, 2013).

The retractable roof of Minute Maid Park in Texas, USA (Figure 1.4(e)) could cover the field with longest span of 132.6 m in length (Smith and Andorka, 2001). Three roof panels are controlled by electro-mechanical drive system to trigger parallel-slide of folding motion along flat crane rails (Riberich, 2000).

Another pivot controlled system of fan-shaped convertible roof structured studio called the Miller Park is constructed was 2001 (Figure 1.4(f)). The total span of 183 m in length of retractable roof which consists of five movable panels that could open and close simultaneously in sweeping manner by rolling along the periphery of heavy wheel (contributors, 2017d, George, 2011, Moser, 2001, Janberg, 2001).

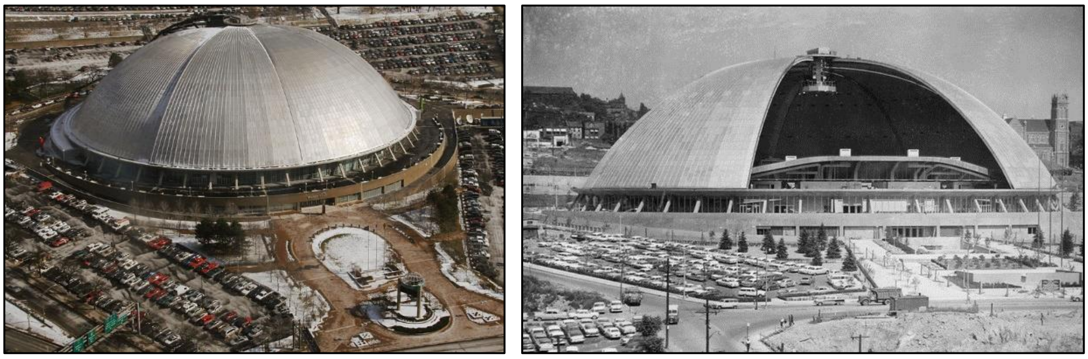

(a) Civic Arena in Pittsburgh, Pennsylvania (Cojo, 2017, Jensen, 2015)

(b) Montreal Olympic Stadium in Quebec, Canada (archINFORM, 2017, Martes, 2013)

(c) Umbrellas for the Piazza of the Prophet´s Holy Mosque, Medina (Soto, 2017)

Figure 1.4- Some Applications of Foldable Roof Structures

(d) Jaén Auditorium in Jaén, Spain (Escrig, 1999)

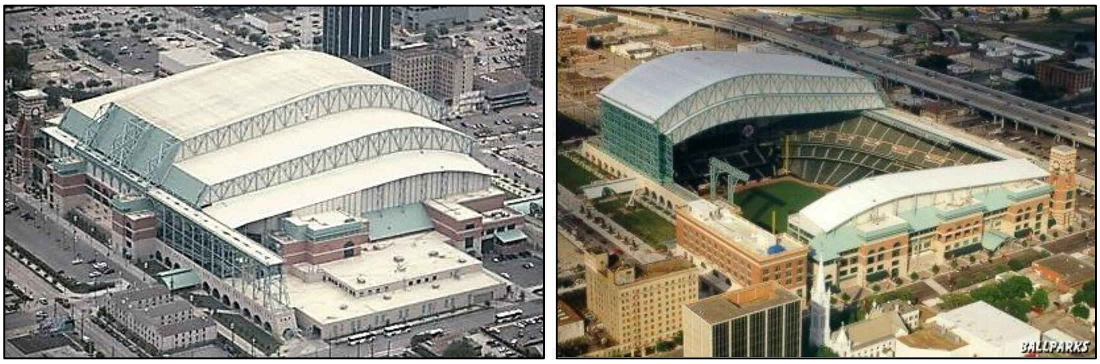

(e) Minute Maid Park Roof in Texas, USA (Riberich, 2000, Smith and Andorka, 2001)

(f) Miller Park in Wisconsin, USA (George, 2011, Moser, 2001)

Figure 1.4- Continued

1.3 Structures Inspired from the Geometry of Origami

Origami or folding paper is a traditional cultural of ancient Chinese and Japanese art of folding paper to represent real objects. Specifically, the word of “origami” comes from Japanese, it is the combination “ori” (root verb “oru”) meaning to fold, and “kami” means for paper (Demaine and O’Rourke, 2007, contributors, 2017b). There are many attempts in classifying types of origami in the world by Center (2017), Origami (2017), Zhezhi and Gi (2017). In general, origami could be broadly classified into six type of folding patterns according to its folding technique and the geometrical requirement of the final output shapes (contributors, 2017f). They are the action origami, modular origami, wet-folding, pureland origami, origami tessellations, and kirigami, as illustrated in Figure 1.5.

Origami reveals a rich source of geometric shape for consideration with different type of origami formations. The beauty of paper folding lies in the result of a totally attractive piece of mathematical artwork which is created from a simple, flat sheet of paper by using almost all folds of corners, creases and edges. Due to the aesthetical value possessed to the idea or concept of geometry originated from origami are widely applied in various industrial fields. It ranges from small products such as electronic devices and micro-cellular tube in medication purposes; to large scaling projects such as auditorium, stadium, and solar panels in satellite.

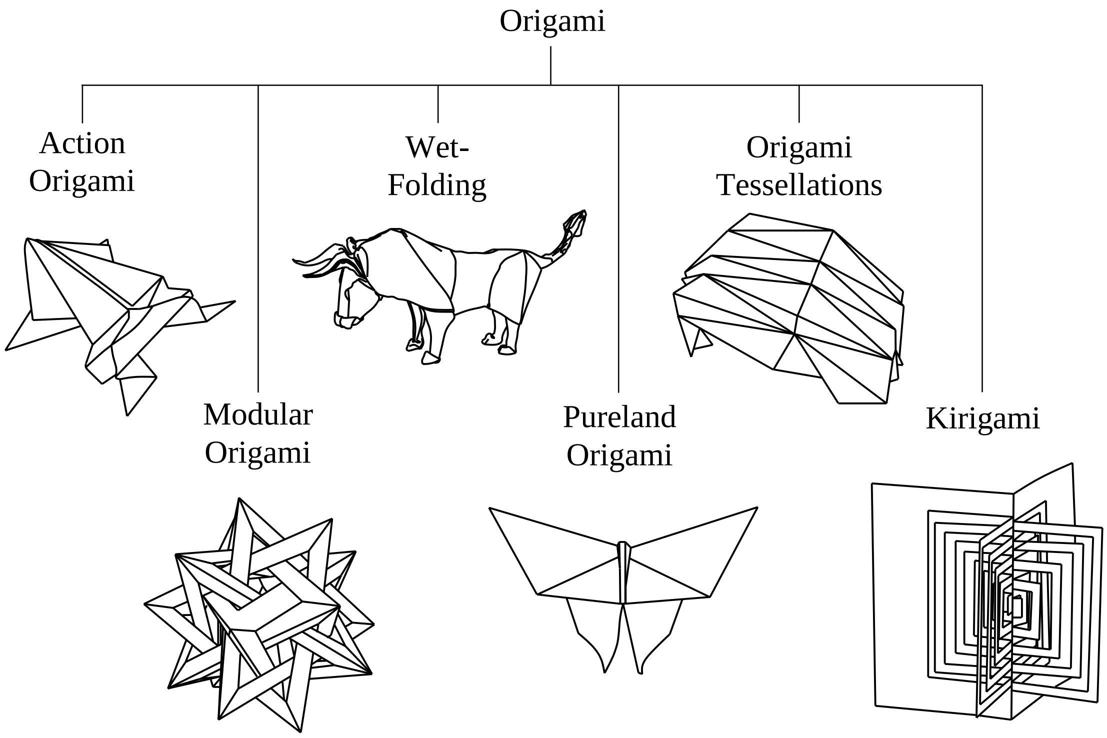

Figure1.5- Type of origami

Forms of geometry created from origami patterns especially the origami tessellations, are nowadays extensively popular in the attempt to implement in large span roof or as foldable structures especially in the form of folded plate or shell. In this context, United States Air Force Academy Cadet Chapel (Figure 1.6(a)) and Yokohama Cruise Terminal in Japan (Figure 1.6(b)) are two well-known examples of shell buildings with folds in which the diagrams and structural relations of origami tessellations can be traced easily. For the Yokohama Cruise Terminal, it could be observed that the internal channel of the terminal is designed using the tessellation type of folding pattern from Yoshimuna technique to create a repetitive diamond effect (FOA, 2006, Mishima and Streeter, 2004).

Figure 1.6(c) shows the Automobile Museum in Nanjing (Figure 1.6(c)), which is inspired by kirigami being constructed in China. The design of the museum combines geometrical idea from spiral-cut of a piece of square paper together with foldings (Basulto, 2010). Besides, another foldable roofing structure that is also inspired by repetitive triangular panels of origami tessellations type called the Bengt Sjostrom Theatre in Rockford, Illinois was built in 2003 (Figure 1.6(d)) (Gang, 2009).

In the practice of architecture it is not surprising to see the impact of origami as a medium to generate different shell forms. Contemporary form is one of the foldable structures that currently being widely employed from the geometrical idea of origami tessellations. In 2008, a foldable artwork called "Packaged" designed by Miwa Takabayashi, which was exhibited in shopping center of Maidstone in Kent, United State (Figure 1.6(e)). It was designed to fold by joining a series of rigid cardboard in the form of tessellation. The artwork was erected in various shopping center as display (Takabayashi, 2009, SORGUÇ et al., 2009).

Another outstanding contemporary pavilion inspired from the origami tessellation of combining two units of "flower" module was designed and built by Tal Friedman in Detmold University, Germany (Figure 1.6(f)). The pavilion is made out of folding rigid aluminum boards. Although, the material used is very thin, it is fully self-supported without any sub-structures. Hence, from the structures inspired by the geometry of origami mentioned above, it could be used to show the potentials of origami as idea for exploring the new form of architectural design in constructing not just large span roofing system, but also for the kinematic requirements as foldable or retractable structures.

(a) United States Air Force Academy Cadet Chapel in Colorado Springs (contributors, 2017g, Harrington, 2017)

(b) Yokohama Cruise Terminal in Japan (Mishima and Streeter, 2004, FOA, 2006)

(c) Automobile Museum in Nanjing, China (Basulto, 2010)

Figure 1.6- Structures Inspired from Geometry of Origami

(d) Bengt Sjostrom Theatre in Rockford, Illinois (Gang, 2009)

(e) “Packaged” Artwork designed by Miwa Takabayashi in Kent, USA (Takabayashi, 2009, SORGUÇ et al., 2009)

(f) Two “Flower” Modules of Origami Pavilion designed by Tal Friedman in Detmold University, Germany (Friedman, 2016)

Figure 1.6- Continued

1.4 Justification of Research

Origami or paper folding is not only a great source of inspiration in architectural design, but also an effective medium for structural form finding because of the foldability characteristic of origami which is useful in the design of shell structure and also foldable or retractable structures. As mentioned earlier in the previous section, straight fold lines are traditionally used. Likewise, by altering the crease and making its configuration into one with curvature, the ordinary planar surface could become a complex 3-D form of which the surface geometry cannot be described easily by simple parameters such as vertex coordinates. Curved folding is a hybrid of curved folds and bending of a paper. The resulting surface is comprised of curved creases and smooth developable surface patches. Comparing with origami with straight fold lines of which the resulting surface consists of folding of rigid planar surface, origami with curved fold lines involves combination of smooth curved surface as a results of bending bounded by set of curved fold lines.

Origami with curved folds could be dated back to early of 1920's, when the teaching works by Josef Albers at Bauhaus was documented in photographs and presented as the first account of a specific curve creased model investigated by Adler (2004). Figure 1.7(a) shows one of the curve creased model that created by a series of concentric circles with alternating mountain and valley folds with a circular hole at the center. Similar features of the model was further explored and modified by Irene Schawinsky in 1944 (McPharlin, 1944) (Figure 1.7(b)), Thoki Yenn in 1989 (Yenn, 2001) (Figure 1.7(c)), and Kunihiko Kasahara in 2002 (Kasahara, 2002) (Figure 1.7(d)). Currently, Erik Demain, Martin Demain and Duks Koschitz are among the most active researches that studying this form of curved crease models (Demaine et al., 2011b, Demaine et al., 1999, Koschitz et al., 2008).

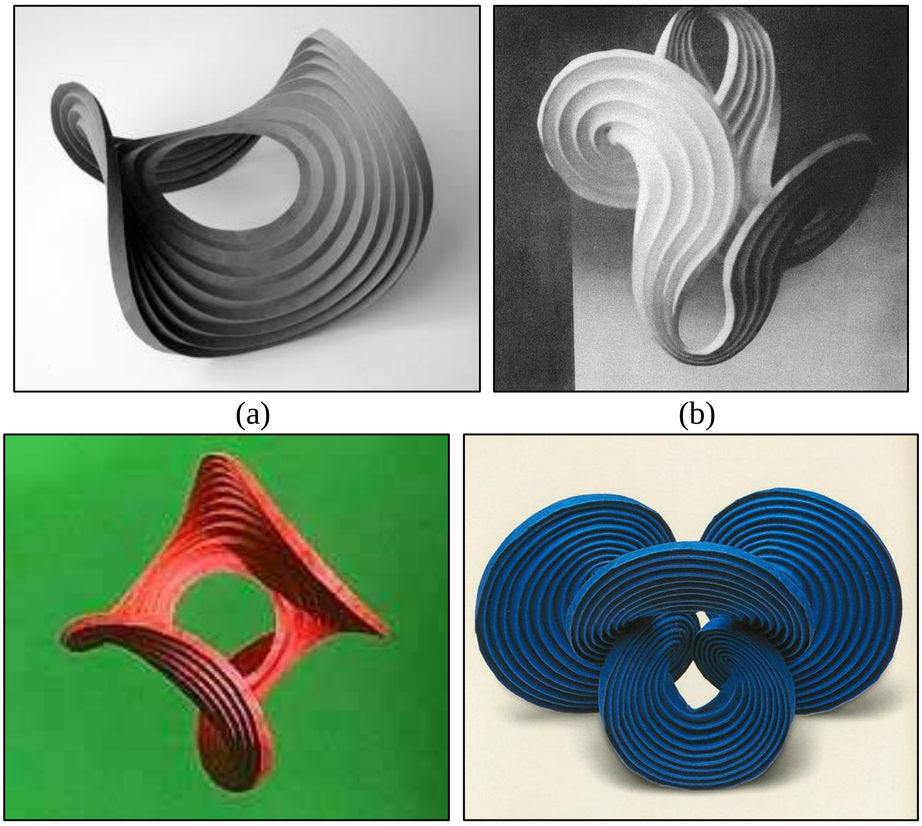

(a) (b) (c) (d)

Figure 1.7- Curve Creased Models: (a) by Josef Albers's students (Schlemmer et al., 1978); (b) by Irene Schawinsky (McPharlin, 1944); (c) by Thoki Yenn (Yenn, 2001); and (d) Kunihiko Kasahara (Kasahara, 2002)

In 1971, Ronald Resch was explored many irregular form of paper folding with curved creases (Resch, 1974). One of the sculpture that he created is called "The White Space Curve Fold with 3-fold Symmetry" as shown in Figure 1.8(a). During almost the same period of time, a mathematician and also a computer scientist, David Huffman, studied in creating paper folding with curve crease based on concept of degree and vertex (Huffman, 1976). Some examples of Huffman's creations are shown in Figure 1.8(b) to Figure 1.8(d) which was documented by Davis et al. (2013) and Demaine et al. (2011a).

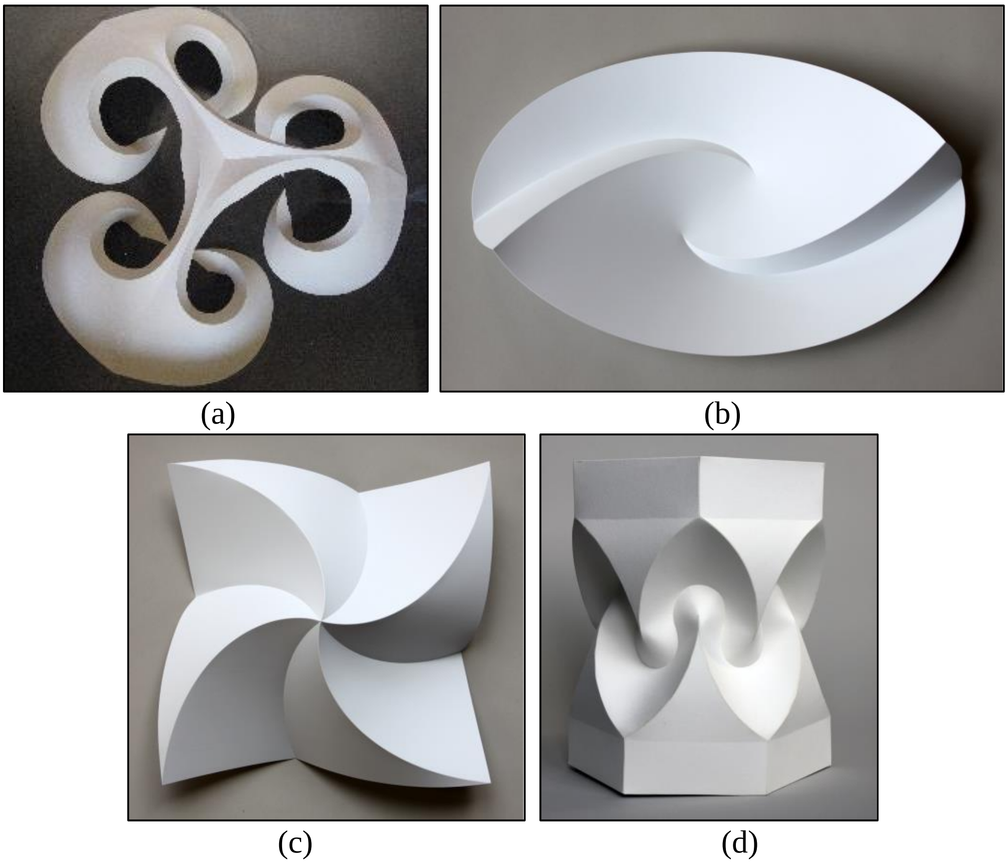

Figure 1.8- Curve Creased Models: (a) “The White Space Curve Fold with 3-fold Symmetry” by Ronald Resch (Resch, 1974); (b) Two Degree-2 Vertices; (c) Non-Inflated Degree-4 Vertex; and (d) “Hexagonal column with cusps” by Huffman (Demaine et al., 2011a)

Another new forms of geometry based on mountain ridged curve folds of origami models were developed by Professor Yoshinobu Miyamoto in 2008 (Miyamoto, 2008, Miyamoto, 2014) as shown in Figure 1.9. In the same year, Kilian et al. (2008) introduced new approach in design and reconstruction of many complex and unexplored origami with curved folds. Apart from the above works on origami with curved fold lines, there were many origami sculptures with curved folds which are created as a contemporary artworks. Most of them are published in webpage for kind of hobby and entertainment, such as those by Chapman-Bell (2010), dimensionaut (2010), Scudellari (2010), Symeonidou (2010a), and Hofmann (2010). Figure 1.10 shows a full picture of historical development of research works in the context of form finding in origami with curved fold lines.

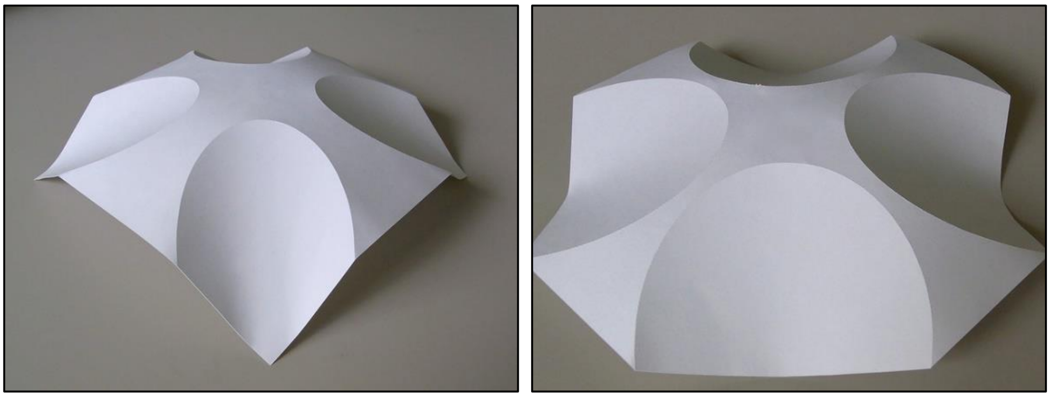

Figure 1.9- Two Examples of origami models with Mountain Ridged Curve Folds by Yoshinobu Miyamoto (Miyamoto, 2008)

A comprehensive exploration on different types of geometrical forms of origami with curved fold lines with different variety of combination of creases and folding patterns has been represented. However, curved folding is still a relatively underexplored topic, when it comes to the aspect of structural application in the discipline of architectural. Therefore, in this research, one of the main goal of the study is to evaluate and identity origami with curved fold lines which possess potential as foldable surface structure. For example, one of Huffman's origami model (Figure 1.11) can be folded (into closed stage) and unfolded (back to open stage), when a gentle force by hands is applied from the corners between folds and boundary of the paper.

1.5 Problem Statement

Origami with straight fold lines typically consists of oblique surface geometry limited with rigid and flat sub-surfaces accompanied with kinking joints. On the other hand, origami with curved fold lines provide instead a three-dimensional smooth curved surface globally where each sub-surfaces between folding joints are bendable. Unique feature of smooth surface geometry embodied in curve folding lines is found mainly in the form of contemporary artwork and creation for entertainment in the form of

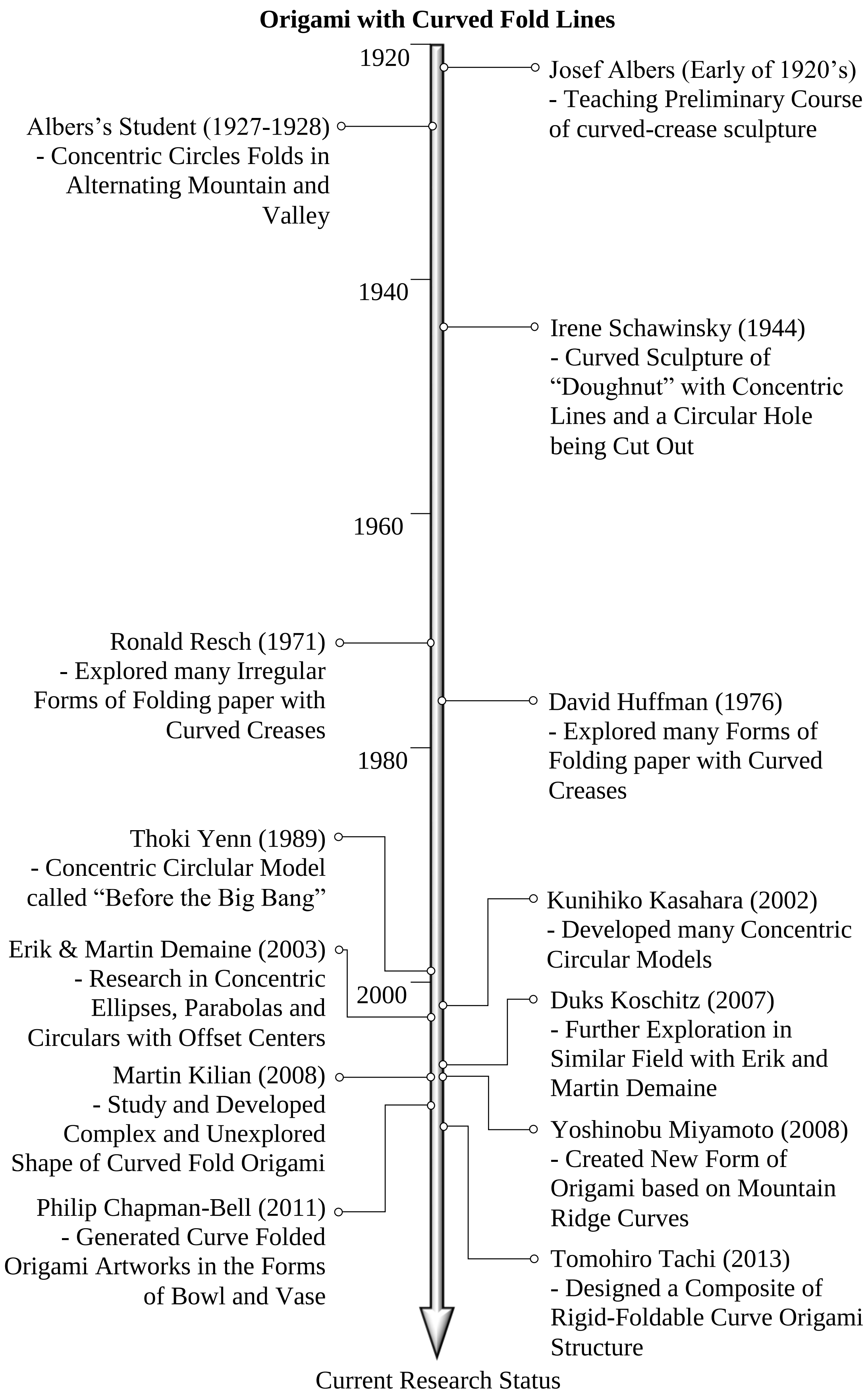

Figure 1.10- The Development of Research Works in the Context of Form Finding in Origami with Curved Fold Lines

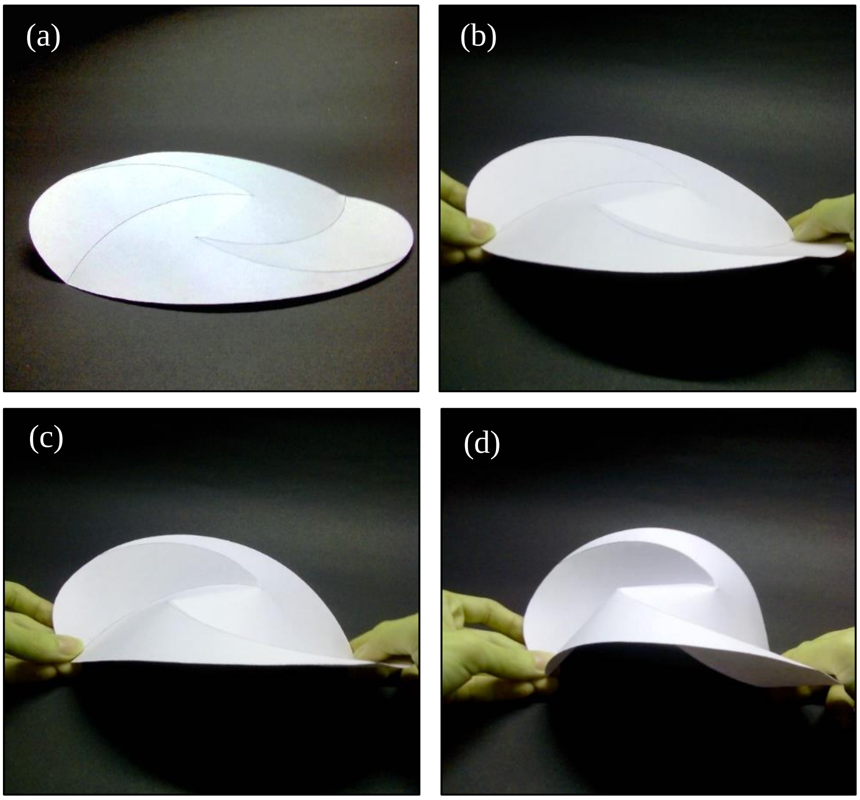

Figure 1.11- Folding Process of Origami Surface with Curved Fold Lines from initial opening-stage of (a) to final closed-stage of (d)

artistic sculptures (Chapman-Bell, 2011, dimensionaut, 2010, Hofmann, 2010, Högsbro, 2010, Miyamoto, 2008, Symeonidou, 2010). Some creations of origami with curved fold lines by pioneers such as Albers (1985) and Huffman (1976) can be used as basis to regenerate the models through preliminary study on the folding patterns and surface configurations (Demaine et al., 2011, Kilian et al., 2008, Koschitz et al., 2008). Unlimited or continuous shape transformation could be achieved with origami with curved fold lines (Schlemmer et al., 1978, McPharlin, 1944, Yenn, 2001, Kasahara, 2002). Although computational simulation on origami shape transformation has been extensively studied (Tachi, 2013, Cai et al., 2013, Schenk, 2009), it is only found within those under straight fold lines. However, in comparison with origami with straight fold lines, potential application of origami with curved fold lines as foldable structure has not attracted much attention. Difficulty in simulating the folding